# Supplementary Lecture Notes for Accelerator Physics

June 2005
Cornell University
Ithaca, NY

William W. MacKay
Brookhaven National Laboratory

Table of Contents

# Canonical Momentum for the Lorentz Force

For a conservative force, the work done by the force in moving from point $P_1$ to point $P_2$ is independent of the path taken:

$$\int_{P_1}^{P_2} \vec{F} \cdot d\vec{r} \quad \text{is invariant,}$$

or more succinctly

$$\oint \vec{F} \cdot d\vec{r} = 0 \tag{1.1}$$

from which by use of Stoke's theorem we get in differential form

$$\nabla \times \vec{F} = 0. \tag{1.2}$$

From basic mechanics we learned that forces which only depend on position and not the velocity of the particle being worked upon are conservative. Examples of such forces are those from gravitational and static electric fields. When there are magnetic fields present the Lorentz force can depend on velocity:

$$\frac{d\vec{p}}{dt} = \vec{F} = q(\vec{E} + \vec{v} \times \vec{B}), \tag{1.3}$$

and is not always conservative. Taking the curl of the Lorentz force yields:

$$
\begin{aligned}
\nabla \times \vec{F} = \nabla \times \frac{d\vec{p}}{dt} &= q(\nabla \times \vec{E} + \nabla \times (\vec{v} \times \vec{B})) \\
&= -q\frac{\partial \vec{B}}{\partial t} + q\left[(\vec{B} \cdot \nabla)\vec{v} - (\vec{v} \cdot \nabla)\vec{B} + (\nabla \cdot \vec{B})\vec{v} - (\nabla \cdot \vec{v})\vec{B}\right] \\
&= -q\frac{\partial \vec{B}}{\partial t} - q\left[(\vec{v} \cdot \nabla)\vec{B}\right] \\
&= -q\left[\frac{\partial \vec{B}}{\partial t} + \frac{\partial \vec{B}}{\partial x}\frac{dx}{dt} + \frac{\partial \vec{B}}{\partial y}\frac{dy}{dt} + \frac{\partial \vec{B}}{\partial z}\frac{dz}{dt}\right] \\
&= -q\frac{d\vec{B}}{dt} \\
&= -\frac{d}{dt}(\nabla \times q\vec{A}).
\end{aligned}
\tag{1.4}
$$

Moving terms to the left side produces

$$\nabla \times \frac{d\vec{p}}{dt} + \frac{d}{dt}(\nabla \times q\vec{A}) = 0, \tag{1.5}$$

which after reordering the differentiation becomes

$$\nabla \times \left[\frac{d}{dt}\left(\vec{p} + q\vec{A}\right)\right] = 0. \tag{1.6}$$

If we define a new *canonical momentum* by

$$\vec{P} = \vec{p} + q\vec{A}, \tag{1.7}$$

then the corresponding *canonical force*

$$\vec{F}_{\text{can}} = \frac{d\vec{P}}{dt} \tag{1.8}$$

is conservative.

# Alternative Derivation of Eq. (CM: 3.75)

In going from Eq. (3.60) to Eq. 3.75 of Conte and MacKay[1], I have not been quite rigorous enough in applying the canonical transformation; hence it was necessary to use a bit of hand waving to add an extra term of $+1$ to the $dz/ds$ equation in Eq. (3.75). When we are more careful with the canonical transformation, we find that the Hamiltonian in Eqs. (3.64 and 3.72) must have an additional term of $+\delta$.

Eq. (3.60) may be rewritten using the paraxial approximation as

$$H_1(x, x', y, y', t, -U/p_0; s) = -\frac{q}{p_0}A_s - \left(1 + \frac{x}{\rho}\right)\sqrt{\left(\frac{U}{p_0 c}\right)^2 - \left(\frac{mc}{p_0}\right)^2 - x'^2 - y'^2}.$$

We would like to transform to a Hamiltonian

$$\mathcal{H}(x, x', y, y', z, \delta; s) = H_1(x, x', y, y', t, -U/p_0; s) + \frac{\partial F_2(t, \delta; s)}{\partial s},$$

where $F_2$ is a generating function for the canonical transformation (See Appendix C.) with

$$z = \frac{\partial F_2}{\partial \delta}, \quad \text{and} \quad -\frac{U}{p_0} = \frac{\partial F_2}{\partial t}.$$

Since

$$\delta = \frac{\Delta p}{p_0} = \frac{U_0^2}{p_0^2 c^2}\frac{\Delta U}{U_0} = \frac{1}{\beta_0^2}\frac{\Delta U}{U_0},$$

the relation between $\frac{U}{p_0}$ and $\delta$ is

$$\frac{U}{p_0} = \frac{c}{\beta}(1 + \beta^2\delta).$$

A good candidate for the generating function is

$$\begin{aligned}
F_2(t, \delta; s) &= \frac{U}{p_0}(t_0 - t) - \frac{s}{\beta_0^2} + s \\
&= \frac{c}{\beta_0}(1 + \beta_0^2\delta)(t_0 - t) - \frac{s}{\beta_0^2} + s \\
&= \frac{c}{\beta_0}(1 + \beta_0^2\delta)\left(\frac{s}{v_0} - t\right) - \frac{s}{\beta_0^2} + s,
\end{aligned}$$

since $s = v_0 t_0$. Evaluating for $z$ then gives

$$z = s - v_0 t,$$

as shown in Eq.(3.63). The additional term missing from Eq. (3.72) is then

$$\frac{\partial F_2}{\partial s} = \delta + 1.$$

Thus we see that a more careful treatment leads to the desired answer without the extra hand waving.

<center>References for Chapter 2</center>

[1] M. Conte and W. W. MacKay, *An Introduction to the Physics of Particle Accelerators*, World Scientific, Singapore (1991).

# Matrix Elements: Synchrobetatron Coupling

For a charged particle of charge $q$ in an external electromagnetic field, we may write the relativistic Hamiltonian as

$$\mathcal{H}(x, P_x, y, P_y, z, P_z; t) = U = \sqrt{(\vec{P} - \vec{A})^2 + m^2 c^4} + q\Phi, \tag{3.1}$$

with vector potential $\vec{A}$, and electric potential $\Phi$, canonical momentum $\vec{P} = \vec{p} + q\vec{A}$, and total energy $U$. Here the kinetic momentum $\vec{p} = \gamma \vec{\beta} mc$. In the usual cylindrical coordinates of accelerator physics with radius of curvature $\rho$, the Hamiltonian may be written as

$$\mathcal{H}(x, P_x, y, P_y, s, P_s; t) = U$$
$$= c\sqrt{(P_x - qA_x)^2 + (P_y - qA_y)^2 + \left(\frac{P_s - qA_s}{1 + x/\rho}\right)^2 + m^2 c^2} + q\Phi. \tag{3.2}$$

Recalling that a canonical transformation from variables $(\vec{q}, \vec{p})$ to variables $(\vec{Q}, \vec{P})$ preserves the Poincaré-Cartan integral invariant

$$\vec{p} \cdot d\vec{q} - H\, dt = \vec{P} \cdot d\vec{Q} - K\, dt, \tag{3.3}$$

we can interchange one canonical pair $(q_j, p_j)$ with the time and energy pair $(t, -H)$ by writing the invariant as

$$\left(\sum_{i \neq j} p_i dq_i + (-H)dt\right) - (-p_j)dq_j. \tag{3.4}$$

This transformation gives the new Hamiltonian

$$\mathrm{H}(x, P_x, y, P_y, t, -U; s) = -P_s$$
$$= -qA_s$$
$$- \left(1 + \frac{x}{\rho}\right)\sqrt{\left(\frac{U - q\Phi}{c}\right)^2 - (mc)^2 - (P_x - qA_x)^2 - (P_y - qA_y)^2}. \tag{3.5}$$

If there are no electrostatic fields then we may write $\Phi = 0$; the fields in rf cavities may be obtained from the time derivative of $\vec{A}$. Ignoring solenoids for now, with only transverse magnetic guide fields and the longituindal electric fields of the cavities, then it is sufficient to have only $A_s$, so

$$A_x = 0, \quad A_y = 0, \quad \text{and} \quad \Phi = 0. \tag{3.6}$$

For dipoles, quadrupoles and cavities a vector potential of the form

$$qA_s = q\left(1 + \frac{x}{\rho}\right)(\vec{A} \cdot \hat{s})$$
$$= -\frac{p_{\mathrm{sy}}}{\rho} x - \frac{p_{\mathrm{sy}} K}{2}(x^2 - y^2) + \dots$$
$$+ \frac{qV}{\omega_{\mathrm{rf}}} \sum_{j=-\infty}^{\infty} \delta(s - jL)\cos(\omega_{\mathrm{rf}} t + \phi_0). \tag{3.7}$$

is sufficient. Here the circumference is $L$, and the magnetic guide field paremeter is

$$K = \frac{1}{\rho^2} + \frac{q}{p_{\text{sy}}} \left( \frac{\partial B}{\partial x} \right)_0, \tag{3.8}$$

and $p_{\text{sy}}$ is the momentum of the synchronous design particle. The effective rf phase as the synchronous particle passes the cavites is $\phi_0$, to give a net energy gain per turn of $[qV \cos(\phi_0)]$. In Eq. (3.7) the effect of all rf cavities has been lumped at the location $s = 0$ in the ring.

The time coordinate may be broken up into the time for the synchronous particle to arrive at the location $s$ plus a deviation $\Delta t$ for the particular particle's arrival time:

$$t = t_{\text{sy}}(s) + \Delta t(s) = \frac{2\pi h}{\omega_{\text{rf}} L} s + \Delta t = \frac{s}{\beta c} + \Delta t. \tag{3.9}$$

If the beam is held at constant energy, then we may make a canonical transformation of the time coordinate $\Delta t$ to rf phase $\varphi$ given by

$$\varphi = \omega_{\text{rf}} \Delta t. \tag{3.10}$$

If acceleration is assumed to be adiabatically slow, so that $\omega_{\text{rf}}$ changes very slowly, and the magnetic guide fields track the momentum of the synchronous particle, keeping the synchronous particle on a fixed trajectory, we can allow for an adiabatic energy ramp according to

$$U_{\text{sy}} = U_0 + \frac{qV \sin \phi_0}{L} s, \tag{3.11}$$

where the energy gain per turn $[qV \sin \phi_0]$ is much less than the total energy $U_s$. In this case it might not unreasonable to use $\varphi$ as the longitudinal coordinate, so long as we are prepared to allow for adiabatic damping of the phase space areas. To convert the time coordinate into an rf phase angle relative to the phase of the synchronous particle, we can use the generating function

$$F_2(x, p_x, t, W; s) = x p_x + \left[ \omega_{\text{rf}} W - \left( U_0 + \frac{qV \sin \phi_0}{L} s \right) \right] t$$
$$- \frac{2\pi h}{L} W s + \frac{qV \pi h \sin \phi_0}{\omega_{\text{rf}} L^2} s^2, \tag{3.12}$$

to find a new canonical momentum $W$ cooresponding to the phase coordinate. This is what was used to arrive at Eq. 7.61 of Ref. [1].*

Before proceeding down this path it will behoove us to examine the effect of ramping the energy. The deviation in energy of another particle of energy $U$ from the synchronous particle may be defined as

$$\Delta U = U - U_{\text{sy}}. \tag{3.13}$$

For the synchronous particle the phase of the rf cavity should be

$$\phi_{\text{sy}} = \phi_0 + \int_0^{t_{\text{sy}}} \omega_{\text{rf}} \, dt$$
$$= \phi_0 + \int_0^{t_{\text{sy}}} \frac{2\pi h \beta c}{L} \, dt_{\text{sy}} \tag{3.14}$$

---

* In writing § 7.6 of Ref. [1], I was following the formalism of Suzuki[2].

With changing energy and the velocity dependance of $\omega_{\mathrm{rf}}$, calculation of this integral becomes a problem and $\varphi$ does not appear to be such an attractive candidate for a canonical coordinate. This is why Chris Iselin chose to take $\zeta = -c\Delta t$ as the longitudinal coordinate variable in the MAD program[3]. Of course there are other parameters which are not necessarily constants in real accelerators. It is quite common to vary the radial position of the closed orbit, as well as the synchronous phase of the rf – particularly during the phase jump at transition crossing. Pulsed quadrupoles are frequently used to cause a rapid change in the transition energy at transition during acceleration.

If we consider a ramp with a constant increase of energy per turn

$$U_{\mathrm{sy}} = U_0 + Rs \quad \text{with}$$
$$R = \frac{qV}{L}\sin\phi_0, \tag{3.15}$$

then the time evolution as a function of path length of the synchronous particles is given by

$$
\begin{aligned}
t_{\mathrm{sy}}(s) &= \int_0^s \frac{ds}{\beta c} \\
&= \int_0^s \left[ 1 - \left( \frac{mc^2}{U_0 + Rs'} \right)^2 \right]^{1/2} ds' \\
&= \frac{mc^2}{R} \int_{\frac{U_0}{mc^2}}^{\frac{U_0+Rs}{mc^2}} \sqrt{1 - \xi^{-2}}\, d\xi, && s' = \frac{\xi mc^2 - U_0}{R} \\
&= -\frac{mc^2}{R} \int_{\frac{mc^2}{U_0}}^{\frac{mc^2}{U_0+Rs}} \sqrt{1 - \eta^2}\, \frac{d\eta}{\eta^2}, && \xi = \frac{1}{\eta} \\
&= \frac{mc^2}{R} \int_{\cos^{-1}\left(\frac{mc^2}{U_0}\right)}^{\cos^{-1}\left(\frac{mc^2}{U_0+Rs}\right)} \tan^2\theta\, d\theta, && \eta = \cos\theta \\
&= \frac{mc^2}{R} \left[\tan\theta - \theta\right]\Bigg|_{\cos^{-1}\left(\frac{mc^2}{U_0}\right)}^{\cos^{-1}\left(\frac{mc^2}{U_0+Rs}\right)} \\
&= \frac{mc^2}{2R} \left[ \frac{U_0 + Rs}{mc^2} \sqrt{1 - \left(\frac{mc^2}{U_0 + Rs}\right)^2} - \frac{U_0}{mc^2}\sqrt{1 - \left(\frac{mc^2}{U_0}\right)^2} \right. \\
&\qquad \left. + \cos^{-1}\left(\frac{mc^2}{U_0 + Rs}\right) - \cos^{-1}\left(\frac{mc^2}{U_0}\right) \right] \\
&= \frac{mc^2}{2R}\left[\beta\gamma - \beta_0\gamma_0 + \cos^{-1}\left(\frac{1}{\gamma}\right) - \cos^{-1}\left(\frac{1}{\gamma_0}\right)\right] \tag{3.16}
\end{aligned}
$$

Provided that the ramping is sufficiently slow, then acceleration may be treated adiabatically.

At least in the adiabatic case, then we can find the new canoncial coordinate and Hamiltonian from Eq. (3.12):

$$-U = \frac{\partial F_2}{\partial t} = \omega_{\mathrm{rf}}W - \left(U_0 + \frac{qV\sin\phi_0}{L}s\right) \tag{3.17a}$$

$$\varphi = \frac{\partial F_2}{\partial W} = \omega_{\mathrm{rf}}t - \frac{2\pi h}{L}s \tag{3.17b}$$

$$\frac{\partial F_2}{\partial s} = -\frac{qV\sin\phi_0}{L}\,t - \frac{2\pi h}{L}\,s + \frac{2\pi h q V\sin\phi_0}{\omega_{\rm rf}L^2}\,s$$

$$= -\frac{qV\sin\phi_0}{L}\left[\frac{2\pi h}{\omega_{\rm rf}L}\,s + \Delta t\right] - \frac{2\pi h}{L}\,s + \frac{2\pi h q V\sin\phi_0}{\omega_{\rm rf}L^2}\,s$$

$$= -\frac{qV\sin\phi_0}{L}\,\frac{\varphi}{\omega_{\rm rf}} - \frac{2\pi h}{L}\,s$$

$$= -\frac{qV\sin\phi_0}{L}\,\frac{\varphi}{\omega_{\rm rf}} - \frac{s}{\lambda_{\rm rf}} \tag{3.17c}$$

Ignoring the vertical coordinate and momentum the new Hamiltonian is

$$H_1(x, p_x, \varphi, W; s) = {\rm H} + \frac{\partial F_2}{\partial s}$$

$$= \frac{p_{\rm sy}}{\rho}\,x + \frac{p_{\rm sy}K}{2}\,x^2 + \frac{qV}{\omega_{\rm rf}}\sum_{j=-\infty}^{\infty}\delta(s - jL)\cos\left(\phi_0 + \varphi + \frac{s}{\lambda_{\rm rf}}\right)$$

$$- \left(1 + \frac{x}{\rho}\right)\left[\frac{(U_{\rm sy} - \omega_{\rm rf}W)^2 - m^2c^4}{c^2} - p_x^2\right]^{1/2} - \frac{qV\sin\phi_0}{L}\,\frac{\varphi}{\omega_{\rm rf}} - \frac{s}{\lambda_{\rm rf}}$$

$$= \frac{p_{\rm sy}}{\rho}\,x + \frac{p_{\rm sy}K}{2}\,x^2 + \frac{qV}{\omega_{\rm rf}}\sum_{j=-\infty}^{\infty}\delta(s - jL)\cos\left(\phi_0 + \varphi + \frac{s}{\lambda_{\rm rf}}\right)$$

$$- \left(1 + \frac{x}{\rho}\right)\left[p_{\rm sy}^2 - \frac{2\omega_{\rm rf}U_{\rm sy}}{c^2}W + \frac{\omega_{\rm rf}^2}{c^2}W^2 - p_x^2\right]^{1/2} - \frac{qV\sin\phi_0}{L}\,\frac{\varphi}{\omega_{\rm rf}} - \frac{s}{\lambda_{\rm rf}}$$

$$\simeq \frac{p_{\rm sy}}{\rho}\,x + \frac{p_{\rm sy}K}{2}\,x^2 + \frac{qV}{\omega_{\rm rf}}\sum_{j=-\infty}^{\infty}\delta(s - jL)\cos\left(\phi_0 + \varphi + \frac{s}{\lambda_{\rm rf}}\right)$$

$$- p_{\rm sy}\left(1 + \frac{x}{\rho}\right)\left[1 - \frac{\omega_{\rm rf}U_{\rm sy}}{p_{\rm sy}^2c^2}W + \left(\frac{\omega_{\rm rf}^2}{2p_{\rm sy}^2c^2} - \frac{1}{8}\frac{4U_{\rm sy}^2\omega_{\rm rf}^2}{p_{\rm sy}^4c^4}\right)W^2 - \frac{1}{2}\frac{p_x^2}{p_{\rm sy}^2}\right]$$

$$- \frac{qV\sin\phi_0}{L}\,\frac{\varphi}{\omega_{\rm rf}} - \frac{s}{\lambda_{\rm rf}}$$

$$\simeq p_{\rm sy}\left\{-1 + \frac{K}{2}\,x^2 + \frac{qV}{\omega_{\rm rf}p_{\rm sy}}\sum_{j=-\infty}^{\infty}\delta(s - jL)\cos\left(\phi_0 + \varphi + \frac{s}{\lambda_{\rm rf}}\right)\right.$$

$$\left. + \left(1 + \frac{x}{\rho}\right)\left[\frac{\omega_{\rm rf}U_{\rm sy}}{p_{\rm sy}^2c^2}W + \frac{m^2\omega_{\rm rf}^2}{2p_{\rm sy}^4}W^2 + \frac{1}{2}\frac{p_x^2}{p_{\rm sy}^2}\right] - \frac{qV\sin\phi_0}{Lp_{\rm sy}}\,\frac{\varphi}{\omega_{\rm rf}} - \frac{s}{\lambda_{\rm rf}}\right\}$$

$$\simeq p_{\rm sy}\left\{-1 + \frac{K}{2}\,x^2 + \frac{qV}{\omega_{\rm rf}p_{\rm sy}}\sum_{j=-\infty}^{\infty}\delta(s - jL)\cos\left(\phi_0 + \varphi + \frac{s}{\lambda_{\rm rf}}\right)\right.$$

$$\left. + \left(1 + \frac{x}{\rho}\right)\left[\frac{1}{\lambda_{\rm rf}}\frac{W}{p_{\rm sy}} + \frac{1}{\gamma^2\lambda_{\rm rf}^2}\left(\frac{W}{p_{\rm sy}}\right)^2 + \frac{1}{2}\left(\frac{p_x}{p_{\rm sy}}\right)^2\right]\right.$$

$$\left. - \frac{qV\sin\phi_0}{Lp_{\rm sy}}\,\frac{\varphi}{\omega_{\rm rf}} - \frac{s}{\lambda_{\rm rf}}\right\} \tag{3.18}$$

This is essentially the same as Eq. (7.61) of Ref. [1] where the longitudinal variables are

$$\varphi = \omega_{\rm rf}\,\Delta t, \quad \text{and} \tag{3.19a}$$

$$W = -\frac{\Delta U}{\omega_{\rm rf}}, \tag{3.19b}$$

$L$ is the circumference, and for magnets with transverse fields and no horizontal-vertical coupling

$$K = \frac{1}{\rho^2} + \frac{q}{p}\left(\frac{\partial B}{\partial x}\right)_0. \tag{3.20}$$

If we want to calculate matrices for the basic magnetic elements, i. e., normal quads and dipoles, then the summation drops out, since $\delta(s - jL) = 0$ and $V = 0$ away from the rf cavities. Then keeping only terms to second order in the canonical variables we have

$$\begin{aligned}
H_1 &\simeq -p_s + \frac{p_s K}{2}x^2 + \frac{p_x^2}{2p_s} \\
&\quad + \left(\frac{U_{\mathrm{sy}}\omega_{\mathrm{rf}}}{p_{\mathrm{sy}}c^2} - \frac{2\pi h}{L}\right)W + \frac{m^2\omega_{\mathrm{rf}}^2}{2p_{\mathrm{sy}}^3}W^2 + \frac{U_{\mathrm{sy}}\omega_{\mathrm{rf}}}{\rho p_{\mathrm{sy}}c^2}Wx \\
&\simeq -p_{\mathrm{sy}} + \frac{p_{\mathrm{sy}}K}{2}x^2 + \frac{p_x^2}{2p_{\mathrm{sy}}} + \frac{m^2\omega_{\mathrm{rf}}^2}{2p_{\mathrm{sy}}^3}W^2 + \frac{U_{\mathrm{sy}}\omega_{\mathrm{rf}}}{\rho p_{\mathrm{sy}}c^2}Wx, \tag{3.21}
\end{aligned}$$

since the two terms in the coefficient of $W$ cancel. We may rescale the Hamiltonian by $1/p_{\mathrm{sy}}$ getting

$$H_{1.5} \simeq -1 + \frac{K}{2}x^2 + \frac{1}{2}w_x{}^2 + \frac{1}{\gamma^2\lambdabar_{\mathrm{rf}}{}^2}w_\phi^2 + \frac{1}{\rho\lambdabar_{\mathrm{rf}}}w_\phi x, \tag{3.22}$$

with the new canonical momenta

$$w_x = \frac{p_x}{p_{\mathrm{sy}}}, \quad \text{and} \tag{3.23a}$$

$$\begin{aligned}
w_\phi &= \frac{W}{p_{\mathrm{sy}}} = -\frac{\Delta U}{\omega_{\mathrm{rf}}p_{\mathrm{sy}}}. \\
&= -\frac{\frac{\beta\gamma mc^3}{\gamma mc^2}}{\frac{2\pi h\beta c}{L}}\frac{\Delta p}{p_{\mathrm{sy}}} \\
&= -\lambdabar_{\mathrm{rf}}\frac{\Delta p}{p_{\mathrm{sy}}}, \tag{3.23b}
\end{aligned}$$

where $\lambdabar_{\mathrm{rf}} = L/2\pi h$. In this case with $\varphi$ and $w_\phi$ as canonically conjugate the longitudinal emittance would have units of length (meters), just like the horizontal and vertical planes. (Of course this should be obvious since all three emittances would come from the common Hamiltonian $H_{1.5}$.) In the paraxial approximation, we obviously have $w_x \simeq x'$.

### 3.1 Quadrupole Matrix

For a normal quadrupole the last term in Eq. (3.22) vanishes, and we have

$$H_{1.5} \simeq -1 + \frac{k}{2}x^2 + \frac{1}{2}w_x{}^2 + \frac{1}{\gamma^2\lambdabar_{\mathrm{rf}}{}^2}w_\phi^2, \tag{3.24}$$

with

$$k = \frac{q}{p_{\mathrm{sy}}}\left(\frac{\partial B}{\partial x}\right)_0. \tag{3.25}$$

Evaluating for the equations of motion, produces

$$\frac{dx}{ds} = \frac{\partial H_{1.5}}{\partial w_x} = w_x \tag{3.26a}$$

$$\frac{dw_x}{ds} = -\frac{\partial H_{1.5}}{\partial x} = -kx \tag{3.26b}$$

$$\frac{d\varphi}{ds} = \frac{\partial H_{1.5}}{\partial w_\phi} = \frac{1}{\gamma^2 \lambda_{\rm rf}{}^2} w_\phi \tag{3.26c}$$

$$\frac{dw_\phi}{ds} = -\frac{\partial H_{1.5}}{\partial \varphi} = 0 \tag{3.26d}$$

So the infinitesimal matrix of integration should look like

$$\mathbf{I} + \mathbf{G}\,ds = \begin{pmatrix} 1 & ds & 0 & 0 \\ -k\,ds & 1 & 0 & 0 \\ 0 & 0 & 1 & \frac{ds}{\gamma^2 \lambda_{\rm rf}{}^2} \\ 0 & 0 & 0 & 1 \end{pmatrix} \tag{3.27}$$

which has the corresponding generator matrix

$$\mathbf{G}\,ds = \begin{pmatrix} 0 & \frac{1}{\sqrt{k}} & 0 & 0 \\ -\sqrt{k} & 0 & 0 & 0 \\ 0 & 0 & 0 & \frac{1}{\gamma^2 \lambda_{\rm rf}{}^2 \sqrt{k}} \\ 0 & 0 & 0 & 0 \end{pmatrix} \sqrt{k}\,ds \tag{3.28}$$

Integration leads to the quadrupole transfer matrix

$$\mathbf{M} = \begin{pmatrix} \cos(\sqrt{k}l) & \frac{1}{\sqrt{k}}\sin(\sqrt{k}l) & 0 & 0 \\ -\sqrt{k}\sin(\sqrt{k}l) & \cos(\sqrt{k}l) & 0 & 0 \\ 0 & 0 & 1 & \frac{l}{\gamma^2 \lambda_{\rm rf}{}^2} \\ 0 & 0 & 0 & 1 \end{pmatrix}. \tag{3.29}$$

**3.2 Drift Matrix**

For a drift $k = 0$ and Eq. (3.27) becomes

$$\mathbf{I} + \mathbf{G}\,ds = \begin{pmatrix} 1 & ds & 0 & 0 \\ 0 & 1 & 0 & 0 \\ 0 & 0 & 1 & \frac{ds}{\gamma^2 \lambda_{\rm rf}{}^2} \\ 0 & 0 & 0 & 1 \end{pmatrix}, \tag{3.30}$$

and leads to the full matrix

$$\mathbf{M} = \begin{pmatrix} 1 & l & 0 & 0 \\ 0 & 1 & 0 & 0 \\ 0 & 0 & 1 & \frac{l}{\gamma^2 \lambda_{\rm rf}{}^2} \\ 0 & 0 & 0 & 1 \end{pmatrix}. \tag{3.31}$$

### 3.3 Sector Bend Matrix

$$K = \frac{1}{\rho^2} + \frac{1}{\rho^2}\frac{\rho}{B_0}\left(\frac{\partial B}{\partial x}\right)_0$$

$$= \frac{1-n}{\rho^2} \tag{3.32}$$

where $n$ is the field index.

$$H_{1.5} \simeq -1 + \frac{1-n}{2\rho^2}x^2 + \frac{1}{2}{w_x}^2 + \frac{1}{2\gamma^2{\lambdabar_{\mathrm{rf}}}^2}w_\phi^2 + \frac{1}{\rho\lambdabar_{\mathrm{rf}}}w_\phi x, \tag{3.33}$$

$$\frac{dx}{ds} = \frac{\partial H_{1.5}}{\partial w_x} = w_x \tag{3.34a}$$

$$\frac{dw_x}{ds} = -\frac{\partial H_{1.5}}{\partial x} = -\frac{1-n}{\rho^2}x - \frac{1}{\rho\lambdabar_{\mathrm{rf}}}w_\phi \tag{3.34b}$$

$$\frac{d\varphi}{ds} = \frac{\partial H_{1.5}}{\partial w_\phi} = \frac{1}{\gamma^2{\lambdabar_{\mathrm{rf}}}^2}w_\phi + \frac{1}{\rho\lambdabar_{\mathrm{rf}}}x \tag{3.34a}$$

$$\frac{dw_\phi}{ds} = -\frac{\partial H_{1.5}}{\partial \varphi} = 0 \tag{3.34a}$$

$$\mathbf{I} + \mathbf{G}\,ds = \begin{pmatrix} 1 & ds & 0 & 0 \\ -\frac{1-n}{\rho^2}ds & 1 & 0 & -\frac{1}{\rho\lambdabar_{\mathrm{rf}}}ds \\ \frac{1}{\rho\lambdabar_{\mathrm{rf}}}ds & 0 & 1 & \frac{1}{\gamma^2{\lambdabar_{\mathrm{rf}}}^2}ds \\ 0 & 0 & 0 & 1 \end{pmatrix} \tag{3.35}$$

$$\mathbf{G} = \frac{1}{\rho}\begin{pmatrix} 0 & \rho & 0 & 0 \\ -\frac{1-n}{\rho} & 0 & 0 & -\frac{1}{\lambdabar_{\mathrm{rf}}} \\ \frac{1}{\lambdabar_{\mathrm{rf}}} & 0 & 0 & \frac{\rho}{\gamma^2{\lambdabar_{\mathrm{rf}}}^2} \\ 0 & 0 & 0 & 0 \end{pmatrix} \tag{3.36a}$$

$$\mathbf{G}^2 = \frac{1}{\rho^2}\begin{pmatrix} -(1-n) & 0 & 0 & -\frac{\rho}{\lambdabar_{\mathrm{rf}}} \\ 0 & -(1-n) & 0 & 0 \\ 0 & \frac{\rho}{\lambdabar_{\mathrm{rf}}} & 0 & 0 \\ 0 & 0 & 0 & 0 \end{pmatrix} \tag{3.36b}$$

$$\mathbf{G}^3 = \frac{1}{\rho^3}\begin{pmatrix} 0 & -\rho(1-n) & 0 & 0 \\ \frac{(1-n)^2}{\rho} & 0 & 0 & \frac{1-n}{\lambdabar_{\mathrm{rf}}} \\ -\frac{1-n}{\lambdabar_{\mathrm{rf}}} & 0 & 0 & -\frac{\rho}{{\lambdabar_{\mathrm{rf}}}^2} \\ 0 & 0 & 0 & 0 \end{pmatrix} \tag{3.36c}$$

$$\mathbf{G}^4 = \frac{1}{\rho^4}\begin{pmatrix} (1-n)^2 & 0 & 0 & \frac{(1-n)\rho}{\lambdabar_{\mathrm{rf}}} \\ 0 & (1-n)^2 & 0 & 0 \\ 0 & -\frac{(1-n)\rho}{\lambdabar_{\mathrm{rf}}} & 0 & 0 \\ 0 & 0 & 0 & 0 \end{pmatrix} = -\frac{1-n}{\rho^2}\mathbf{G}^2. \tag{3.36d}$$

$$\mathbf{M} = \begin{pmatrix} \cos\left[\sqrt{1-n}\theta\right] & \frac{\rho\sin\left[\sqrt{1-n}\theta\right]}{\sqrt{1-n}} & 0 & \frac{\rho\left(1-\cos\left[\sqrt{1-n}\theta\right]\right)}{(1-n)\lambdabar_{\mathrm{rf}}} \\ \frac{\sqrt{1-n}\,\sin\left[\sqrt{1-n}\theta\right]}{\rho} & \cos\left[\sqrt{1-n}\theta\right] & 0 & \frac{\sin\left[\sqrt{1-n}\theta\right]}{\sqrt{1-n}\lambdabar_{\mathrm{rf}}} \\ -\frac{\sin\left[\sqrt{1-n}\theta\right]}{\sqrt{1-n}\lambdabar_{\mathrm{rf}}} & -\frac{\rho\left(1-\cos\left[\sqrt{1-n}\theta\right]\right)}{(1-n)\lambdabar_{\mathrm{rf}}} & 1 & \frac{\rho}{{\lambdabar_{\mathrm{rf}}}^2}\left\{\frac{\theta}{\gamma^2} - \frac{\sqrt{1-n}\theta-\sin\left[\sqrt{1-n}\theta\right]}{(1-n)^{-3/2}}\right\} \\ 0 & 0 & 0 & 1 \end{pmatrix} \tag{3.37}$$

<u>References for Chapter 3</u>

[1] Mario Conte and William W. MacKay, *An Introduction to the Physics of Particle Accelerators*, World Sci., Singapore (1991).

[2] Toshio Suzuki, "Hamiltonian Formulation for Synchrotron Oscillations and SAcherer's Integral Equation", *Particle Accelators*, **12**, 237 (1982).

[3] F. C. Iselin, "Lie Transformations and Transport Equations for Combined-Function Dipoles", *Particle Accelators*, **17**, 143 (1985).

[4]  Milton Abramowitz and Irene Stegun, *Handbook of Mathematical Functions*, Dover Pub., New York (1970).

# 4

# Comments on Canonical Coordinates

## 4.1 Nonparaxial considerations in the transverse plane

The paraxial approximation is generally obtained by dividing the Hamiltonian by the design momentum $p_0$ and making a small angle approximation. In the scale transformation obtained by dividing $H$ by $p_0$ the real transverse momenta conjugate to the $x$ and $y$ coordinates are

$$s_x = \frac{p_x}{p_0} = \sin\theta_x \tag{4.1a}$$

$$s_y = \frac{p_y}{p_0} = \sin\theta_y, \tag{4.1b}$$

where $\theta_x$ and $\theta_y$ are the projections of the trajectory angle with respect to the design orbit. As stated earlier, the approximation is made for small angles by

$$\sin\theta_j \simeq \tan\theta_j$$

. Suppose we would still like to transform the transverse momenta to $x'$ and $y'$ without the paraxial approximation. What canonical coordinates could we expect to find. We need to construct a new $F_2$ function for the canonical transformation. Remember that $F_2(x, x', y, y'; s)$ is a function of old coordinates and new momenta with the partial derivatives:

$$\frac{\partial F_2}{\partial x} = \frac{p_x}{p_0} = x'\sqrt{1 - x'^2 - y'^2} \tag{4.2a}$$

$$\frac{\partial F_2}{\partial y} = \frac{p_x}{p_0} = y'\sqrt{1 - x'^2 - y'^2} \tag{4.2b}$$

$$\frac{\partial F_2}{\partial x'} = q_x \tag{4.2c}$$

$$\frac{\partial F_2}{\partial y'} = q_y. \tag{4.2d}$$

From the first pair of equations we find a good choice for $F_2$ to be

$$F_2(x, x', y, y'; s) = (xx' + yy')\sqrt{1 - x'^2 - y'^2}. \tag{4.3}$$

Evaluating the second pair of equations (4.2a&b) gives:

$$\begin{pmatrix} q_x \\ q_y \end{pmatrix} = \frac{1}{\sqrt{1 - x'^2 - y'^2}} \begin{pmatrix} 1 - 2x'^2 - y'^2 & -x'y' \\ -x'y' & 1 - x'^2 - 2y'^2 \end{pmatrix} \begin{pmatrix} x \\ y \end{pmatrix}. \tag{4.4}$$

Inverting the matrix and solving for the old coordinates yields

$$\begin{pmatrix} x \\ y \end{pmatrix} = \sqrt{1 - x'^2 - y'^2}\frac{1}{D} \begin{pmatrix} 1 - x'^2 - 2y'^2 & x'y' \\ x'y' & 1 - 2x'^2 - y'^2 \end{pmatrix} \begin{pmatrix} q_x \\ q_y \end{pmatrix}, \tag{4.5}$$

where the determinant

$$D = (1 - 2x'^2 - y'^2)(1 - x'^2 - 2y'^2) - x'^2 y'^2$$
$$= [1 - (x'^2 + y'^2)][1 - 2(x'^2 + y'^2)]. \tag{4.6}$$

So the old coordinates in terms of the new ones must be replaced by

$$x = \frac{(1 - x'^2 - 2y'^2)q_x + x'y'q_y}{(1 - x'^2 - y'^2)^{1/2}[1 - 2(x'^2 + y'^2)]} \tag{4.7a}$$

$$y = \frac{x'y'q_x + (1 - 2x'^2 - y'^2)q_y}{(1 - x'^2 - y'^2)^{1/2}[1 - 2(x'^2 + y'^2)]}. \tag{4.7b}$$

This will create one bloody-awful mess, won't it?

If we expand $q_x$ and $q_y$ in power series to $3^{\text{rd}}$ order we obtain

$$q_x = x - \tfrac{1}{2}\left(3x'^2 + y'^2\right)x - x'y'y + \cdots \tag{4.8a}$$

$$q_y = y - \tfrac{1}{2}\left(x'^2 + 3y'^2\right)y - x'y'x + \cdots \tag{4.8b}$$

So if we are only interested in terms up to second order, the paraxial approximation will probably work, but if we want to keep terms to third order or higher, then we should use the canonical momenta $p_x/p_0$ and $p_y/p_0$ rather than $x'$ and $y'$.

## 4.2 Longitudinal coordinates variations

There are a several different combinations for the longintudinal canonical variables, for example:

$$\left(z\;, \tfrac{\Delta p}{p_0}\right) \tag{4.9a}$$

$$\left(-c\,\Delta t, \tfrac{\Delta u}{p_0 c}\right) \tag{4.9b}$$

$$(\phi\;, w_\phi). \tag{4.9c}$$

Differentiating the equation

$$U^2 = p^2 c^2 + m^2 c^4, \tag{4.10a}$$

leads to the relation

$$du = \beta c\, dp, \tag{4.10b}$$

or on converting to fractional deviations

$$\frac{dp}{p_0} = \frac{1}{\beta}\frac{du}{p_0 c} = \frac{1}{\beta^2}\frac{du}{U_0}. \tag{4.11}$$

Conversion from the pair Eq. (4.9a) to pair Eq. (4.9b) used in the MAD[2] program may be accomplished by

$$\begin{pmatrix} z \\ \frac{\Delta p}{p_0} \end{pmatrix} = \begin{pmatrix} -\beta_0 c(t - t_0) \\ \frac{\Delta p}{p_0} \end{pmatrix} = \begin{pmatrix} -\beta_0 c\Delta t \\ \beta_0^{-1}\frac{\Delta u}{p_0 c} \end{pmatrix} = \begin{pmatrix} \beta_0 & 0 \\ 0 & \beta_0^{-1} \end{pmatrix} \begin{pmatrix} -c\Delta t \\ \frac{\Delta u}{p_0 c} \end{pmatrix} \tag{4.12}$$

The usual definition of dispersion gives the particular solution to the inhomogeneous horizontal Hill's equation (Eq. 5.77 of Ref. 2) must be modified by a factor of $\beta$ to agree with the value calculated by MAD.

## References

1. Herbert Goldstein, *Classical Mechanics*, $2^{nd}$ Ed., Addison-Wesley Pub. Co., Reading MA, (1980).

2. Mario Conte and William W. MacKay, An Introduction to the Physics of Particle Accelerators, World Scientific Pub. Co., Singapore (1991).

3. Hans Grote and F. Christoph Iselin, "The MAD Program Userś Reference Manual", CERN/SL/90-13(AP) (Rev. 5) (1996).

4. F. Ch. Iselin, Particle Accelerators, **17**, 143 (1985).

# 5

# Transverse Position Measurement

One of the most common methods for measuring the transverse position of the a bunched beam is to sense the electric field with capacitive pickups. As the bunch travels down the beam pipe, image charges move along the inner surface of the pipe. (Here I am of course assuming that the beam pipe is made of metal.) From Gauss' law it is easy to see that the total charge moving along the pipe must be equal but of opposite sign to the charge in the bunch.
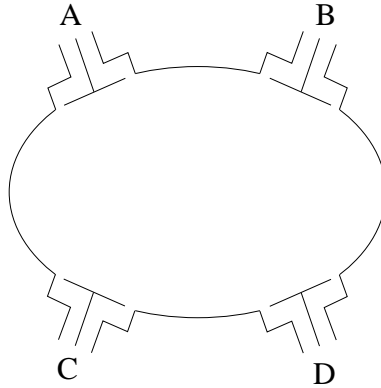


Figure. 5.1 Concept of a dual plane beam-button position monitor. The signals from each button are brought out to the readout electronics via high quality coaxial cables. Here the buttons have been placed as in a synchrotron light source to keep them out of the band of synchrotron radiation in the midplane.

One type monitor employs button shaped electrodes to sense the electric field strength at the surface of the chamber as shown in Fig. (5.1). Buttons are particularly used when the bunches are short as in electron accelerators. The short length of the electrode can limit the amount of induced charge if the bunches are longer than the radius of the button.

When the bunches are longer as in hadron accelerators, longer stripline electrodes are frequently used. Fig. (5.2) shows a shorted stripline monitor with a measured signal from the lower stripline.

An estimate of the charge density on the inner surface of a cylindrical beam pipe of radius $b$ can be made by treating the bunch as a line of charge of density $\lambda$ at a distance $a$ from the center of the pipe. Ignoring the pipe, a second line of image charge (line density: $-R\lambda$) can be placed parallel to the beam but at a distance $A$ from the origin. We solve for distance $A$ and the ratio $R$ to have an equipotential surface on a cylinder of radius $b$. The equation for the potential lines of charge is then
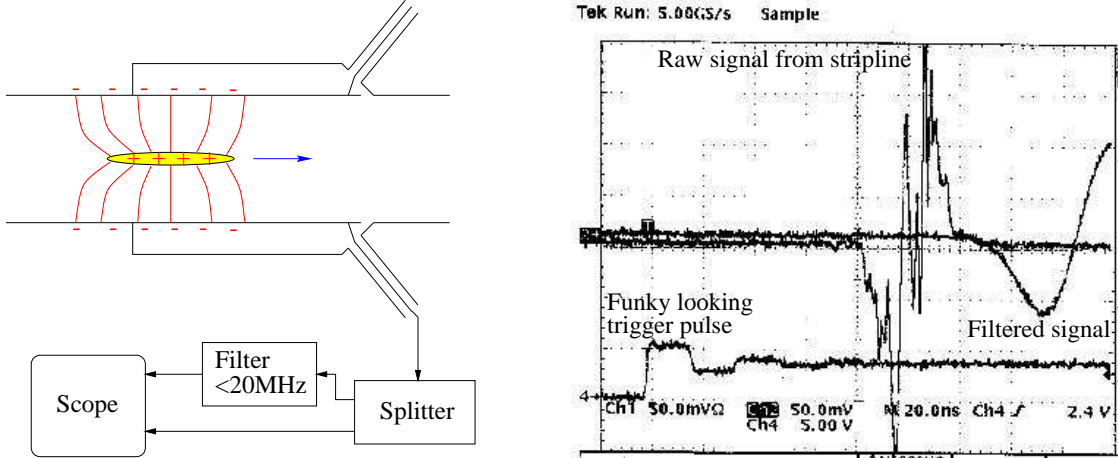
Figure. 5.2 Concept of a stripline beam position monitor. Induced currents on the wall are picked up on coaxial cables by using a small gap at the end of the stripline. The capacitive nature of such a pickup differentiates the bunch current. On the right are measurements of a fully stripped gold bunch passing through a stripline position monitor after being extracted from the AGS. As can be seen, there was quite a bit of structure in the bunch. (This was taken early in the commissioning of the extraction system.)
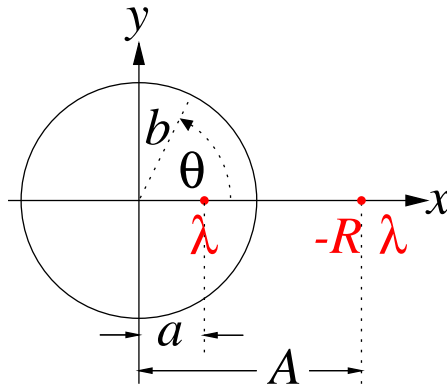


Figure. 5.3 Equipotential surface with line of charge density $\lambda$ at radius $a$ and an image line of charge of density $-R\lambda$ at radius $A$.

$$V = \frac{\lambda}{2\pi\epsilon_0}\left[\ln\left(\sqrt{(x-a)^2+y^2}\right) - R\ln\left(\sqrt{(x-A)^2+y^2}\right)\right] + V_0. \tag{5.1}$$

Rearranging terms produces

$$\frac{2\pi\epsilon_0}{\lambda}(V - V_0) = \frac{1}{2}\ln\frac{(x-a)^2+y^2}{[(x-A)^2+y^2]^R}. \tag{5.2}$$

After exponentiating, we may define

$$\alpha = e^{\frac{4\pi\epsilon_0}{\lambda}(V-V_0)} = \frac{(x-a)^2+y^2}{[(x-A)^2+y^2]^R}. \tag{5.3}$$

In order to have a cylindrical equipotential surface, we must have a quadratic equation, so $R = 1$, and
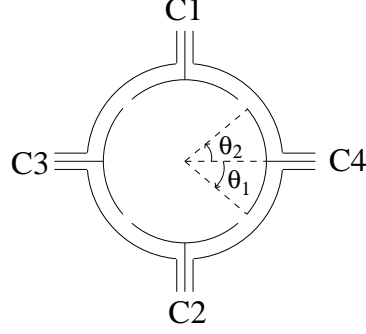
$$(x-a)^2 + y^2 = \alpha[(x-A)^2 + y^2].$$

Figure. 5.4 Definition of angles of integration for stripline "C4".

Since the potential at $(x, y) = (b, 0)$ must be the same as at $(x, y) = (0, b)$, we can write

$$\alpha = \frac{(b - a)^2}{(A - b)^2} = \frac{a^2 + b^2}{A^2 + b^2}. \tag{5.4}$$

Solving for A gives the nontrivial answer

$$A = \frac{b^2}{a}.$$

(The other root is $A = a$ which just cancels the charge at $x = a$.) Transforming to polar coordinates $(x = r \cos\theta, \ y = r \sin\theta)$ and evaluating the radial component of electric field at $r = b$ gives

$$E_r(r = b, \theta) = -\frac{\lambda}{2\pi\epsilon_0} \left[ \frac{b^2 - a^2}{b(b^2 + a^2 - 2ab\cos\theta)} \right]. \tag{5.5}$$

Since the field is zero inside the conductor, the surface on the inner wall of the beam pipe must be

$$\sigma(\theta) = \epsilon_0 E_\perp = -\frac{\lambda}{2\pi} \left[ \frac{b^2 - a^2}{b(b^2 + a^2 - 2ab\cos\theta)} \right]. \tag{5.6}$$

Now the charge per length on a stripline subtending the arc from $\theta_1$ to $\theta_2$ (See Fig. (5.4).) obtained by integrating

$$\frac{dq}{dz} = -\frac{\lambda}{2\pi} \int_{\theta_1}^{\theta_2} \left[ \frac{b^2 - a^2}{b(b^2 + a^2 - 2ab\cos\theta)} \right] d\theta$$

$$= \frac{\lambda}{\pi} \tan^{-1} \left[ \left( \frac{b + a}{b - a} \right) \tan\frac{\theta}{2} \right] \Bigg|_{\theta_1}^{\theta_2}. \tag{5.7}$$

For the opposite plate we can reverse the sign of $a$. The voltage induced across the coaxial cables will be proportional to the $dq/dz$ on the stripline. To go further requires either a lot more algebra or invocation of a symbolic calculator such as MAPLE[3]. To first order in $x/b$ we get

$$\frac{V_1 - V_2}{V_1 + V_2} = 4\frac{\sin\frac{\alpha}{2}}{\alpha} \frac{x}{b} + O\left(\frac{x^3}{b^3}\right) + O\left(\frac{xy^2}{b^3}\right). \tag{5.8}$$

where $\alpha = \theta_2 - \theta_1$, and we have replaced $a$ by $x$. A somewhat more linear formula comes from

$$\ln\frac{V_1}{V_2} = 8\frac{\sin\frac{\alpha}{2}}{\alpha} \frac{x}{b} + O\left(\frac{x^3}{b^3}\right) + O\left(\frac{xy^2}{b^3}\right). \tag{5.9}$$

As an example, assume that the striplines subtend an angle of $\alpha = 70°$ ($\theta_1 = -35°$, $\theta_2 = 35°$) and a radius for the striplines of $b = 56.5$ mm, then we get to first order from Eq. (5.8): Fig. (5.5) shows typical signals from the four plates of a dual plane stripline with above dimensions.
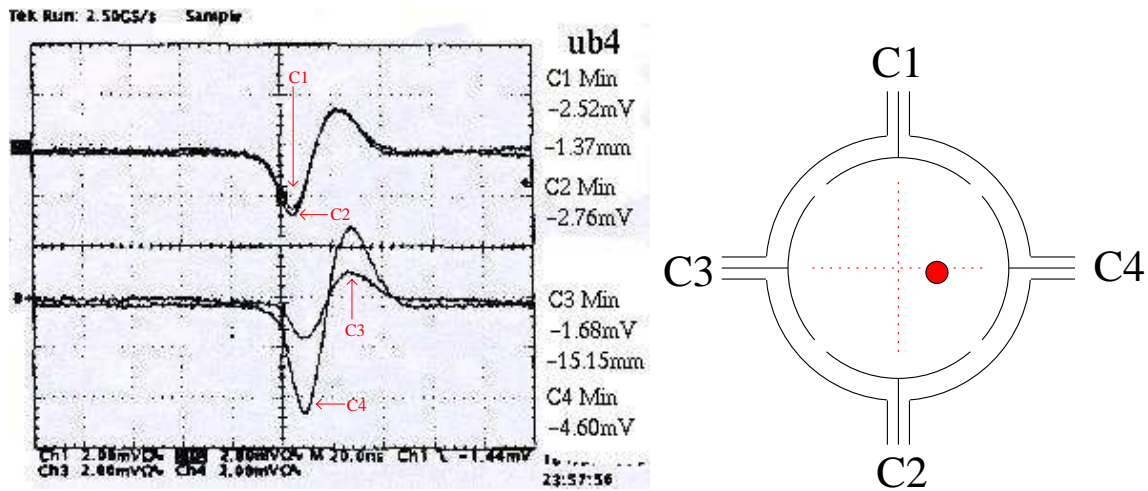


Figure. 5.5 Filtered signals from all four striplines of a two plane position monitor. The relative sizes of the voltages show that the beam was slightly down and to the right as indicated in the picture on the right. The positions were calculated using Eq. (5.9).

The accuracy of relative position measurements in a circular accelerator with a stripline monitor can be better than 10 $\mu$m when the signals are averaged over several turns.

### References for Chapter 5

[1] R. E. Shafer, "Beam Position Monitoring", AIP Conf. Proc. 212, p. 26, New York (1990).

[2] R. E. Shafer, "Characteristics of Directional Coupler Beam Position Monitors", *IEEE Trans. on Nucl. Sci.*, Vol. NS-32, #5 p. 1933 (1985).

[3] B. W. Char et al., *Maple V First Leaves: A Tutorial Introduction* Springer-Verlag, New York (1992)

# 6

# Schottky Signals

## 6.1 Coherent frequency spectra of bunched beams

### 6.1.1 A single Gaussian bunch

A Gaussian bunch of total charge $q$ passing a pickup at location $s$ will have a longitudinal profile

$$dQ(s,t) = \frac{q}{\sqrt{2\pi}\sigma_s} e^{\frac{-(s-vt)^2}{2\sigma_s}} ds, \tag{6.1}$$

where $\sigma_s$ is the rms width of the distribution. The distribution of current passing the pickup is then

$$
\begin{aligned}
i(t) &= \frac{dQ}{dt} = v\frac{dQ}{ds} \\
&= \frac{qv}{\sqrt{2\pi}\sigma_s} e^{\frac{-(s-vt)^2}{2\sigma_s}} \\
&= \frac{q}{\sqrt{2\pi}\sigma_t} e^{\frac{-(t-t_0)^2}{2\sigma_t}},
\end{aligned} \tag{6.2}
$$

where $t_0 = s/v$. For the following discussion, we will place the pickup at $s = 0$, so $t_0 = 0$. The harmonic content of the signal may be found from the Fourier transform[†] of the current:

$$
\begin{aligned}
\hat{i}(\omega) &= \frac{q}{\sqrt{2\pi}\sigma_t} \int_{-\infty}^{\infty} e^{-j\omega t} e^{-\frac{t^2}{2\sigma_t^2}} dt, \\
&= \frac{q}{\sqrt{2\pi}\sigma_t} e^{-\frac{\sigma_t^2\omega^2}{2}} \int_{-\infty}^{\infty} e^{-\frac{(t+j\sigma_t^2\omega)^2}{2\sigma_t^2}} dt, \\
&= q\, e^{-\frac{\sigma_t^2\omega^2}{2}}.
\end{aligned} \tag{6.3}
$$

So we find that the Fourier transform of a Gaussian distribution is again Gaussian with an rms width of $\sigma_\omega = 1/\sigma_t$. In the limit of an infinitesimally short bunch the Gaussian distribution becomes

$$i(t) = \lim_{\sigma_t \to 0} \frac{q}{\sqrt{2\pi}\sigma_t} e^{-\frac{t^2}{2\sigma_t}} = q\,\delta(t), \tag{6.4}$$

and the spectral content becomes flat

$$\hat{i}(\omega) = q \int_{-\infty}^{\infty} e^{-j\omega t}\,\delta(t)\,dt = q. \tag{6.5}$$

---

[†] Here I have used the engineering convention of $j = \sqrt{-1}$ to minimize confusion with the current $i$.

### 6.1.2 Circulating bunches

The bunched beam current in a circular accelerator of circumference $L$ with $N_p$ equally spaced bunches may be approximated by

$$i(t) = \sum_{n=-\infty}^{\infty} \sum_{m=1}^{N_p} \int_{-\infty}^{\infty} Q_m(t') \, \delta\left(t - t' - \frac{nmL}{N_p v}\right) dt', \tag{6.6}$$

where $Q_m(t') = dq_m/dt'$ is the longitudinal profile of charge in the $m^{\text{th}}$ bunch. The frequency spectrum may be obtained from the Fourier transform of the current:

$$\hat{i}(\omega) = \sum_{m=1}^{N_p} \sum_{n=-\infty}^{\infty} \int_{-\infty}^{\infty} \int_{-\infty}^{\infty} e^{-j\omega t} \, Q_m(t') \, \delta\left(t - t' - \frac{nmL}{N_p v}\right) dt' \, dt,$$

$$= \sum_{m=1}^{N_p} \sum_{n=-\infty}^{\infty} \hat{Q}_m(\omega) \exp\left(-j\frac{nmL}{N_p v}\omega\right). \tag{6.7}$$

When the bunches are identical this becomes:

$$\hat{i}(\omega) = \hat{Q}(\omega) \sum_{n=-\infty}^{\infty} \exp\left(-j\frac{nL}{N_p v}\omega\right) = \frac{Q(\omega)}{N_p \omega_s} \sum_{n=-\infty}^{\infty} \delta\left(\omega - nN_p\omega_s\right) \tag{6.8}$$

with $\omega_o = 2\pi v/L$ being the angular revolution frequency.

If we approximate the bunch shape by a delta function, then the spectrum will have a "comb"-shape as shown in Fig. (6.1).
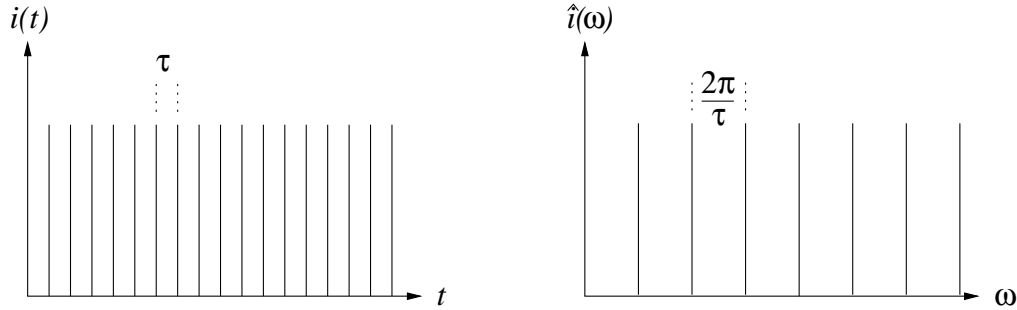


Figure. 6.1 The left plot shows the current distribution for equal $\delta$-function bunches of charge $Q_m(t') = q\delta(t'))$ and spacing $\tau = L/N_p v$. The right plot shows the corresponding Fourier transform.

If we now allow a gap in the number of bunches so that only $N_b$ bunches are placed with the same spacing leaving $N_p - N_b$ holes in the bunch train, we should expect to see additional harmonics of the revolution lines between those of Eq. (6.8). Consider $N_b$ bunches of equal charge $q$ and width $\sigma$ placed in $N_p$ equally spaced buckets:

$$i(t) = \sum_{n=-\infty}^{\infty} \sum_{m=1}^{N_b} \int_{-\infty}^{\infty} \int_{-\infty}^{\infty} e^{-j\omega t} \frac{q}{\sqrt{2\pi}\sigma} e^{-\frac{t'^2}{2\sigma^2}} \, \delta\left(t - t' - \frac{nm}{N_p}\tau_s\right) dt' \, dt. \tag{6.8}$$
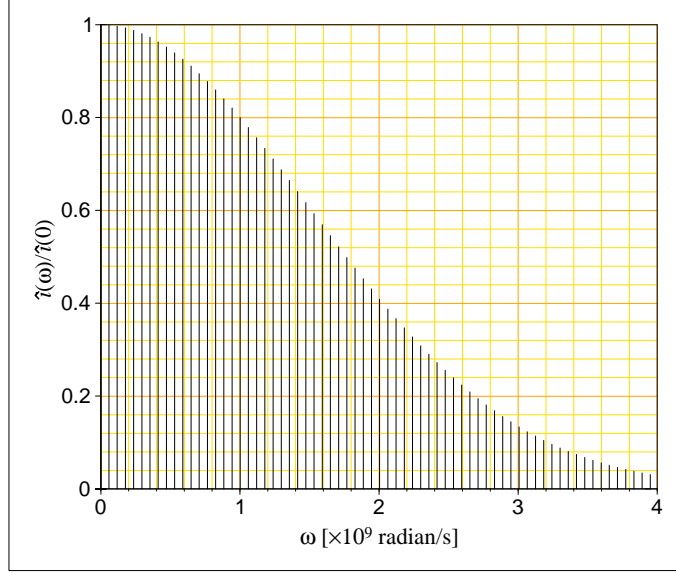
Figure. 6.2 Relative frequency of equal Gaussian bunches with 106.6 ns spacing between bunches.

The frequency spectrum is then

$$
\begin{aligned}
\hat{\imath}(\omega) &= q e^{-\frac{\sigma^2 \omega^2}{2}} \sum_{n=-\infty}^{\infty} \sum_{m=1}^{N_b} \int_{-\infty}^{\infty} e^{-j\omega t}\, \delta\left(t - \frac{nm}{N_p}\tau_s\right) dt \\
&= q e^{-\frac{\sigma^2 \omega^2}{2}} \sum_{n=-\infty}^{\infty} \sum_{m=1}^{N_b} e^{-j\frac{nm\omega\tau_s}{N_p}} \\
&= q e^{-\frac{\sigma^2 \omega^2}{2}} \sum_{n=-\infty}^{\infty} e^{-j\frac{n\omega\tau_s}{N_p}} \frac{1 - e^{-j\frac{nN_b\omega\tau_s}{N_p}}}{1 - e^{-j\frac{n\omega\tau_s}{N_p}}} \\
&= q e^{-\frac{\sigma^2 \omega^2}{2}} \sum_{n=-\infty}^{\infty} e^{-j\frac{n\omega\tau_s}{N_p}} e^{-j\frac{nm\omega\tau_s}{2N_p}} \frac{2j\left(e^{j\frac{nN_b\omega\tau_s}{2N_p}} - e^{-j\frac{nN_b\omega\tau_s}{2N_p}}\right)}{2j\left(e^{j\frac{n\omega\tau_s}{2N_p}} - e^{-j\frac{n\omega\tau_s}{2N_p}}\right)} \\
&= q e^{-\frac{\sigma^2 \omega^2}{2}} \sum_{n=-\infty}^{\infty} \frac{\sin\left(\frac{nN_b\omega\tau_s}{2N_p}\right)}{\sin\left(\frac{n\omega\tau_s}{2N_p}\right)} e^{-j\frac{n(N_b+1)\omega\tau_s}{2N_p}}
\end{aligned}
$$

The modulation factor, called the *enhancement* function, is

$$
\mathcal{E}_n(\omega) = \frac{\sin\left(\frac{nN_b\tau_s}{2N_p}\omega\right)}{\sin\left(\frac{n\tau_s}{2N_p}\omega\right)}. \tag{6.9}
$$

From this we see that having an irregular pattern of bunches will produce more closely spaced lines separated by the revolution frequency $(1/\tau_s)$ which is smaller than the typical bunch frequency $(N_p/\tau_s)$. Other enhancement factors can be calculated for bunches of differing intensity or with more gaps between bunch trains.
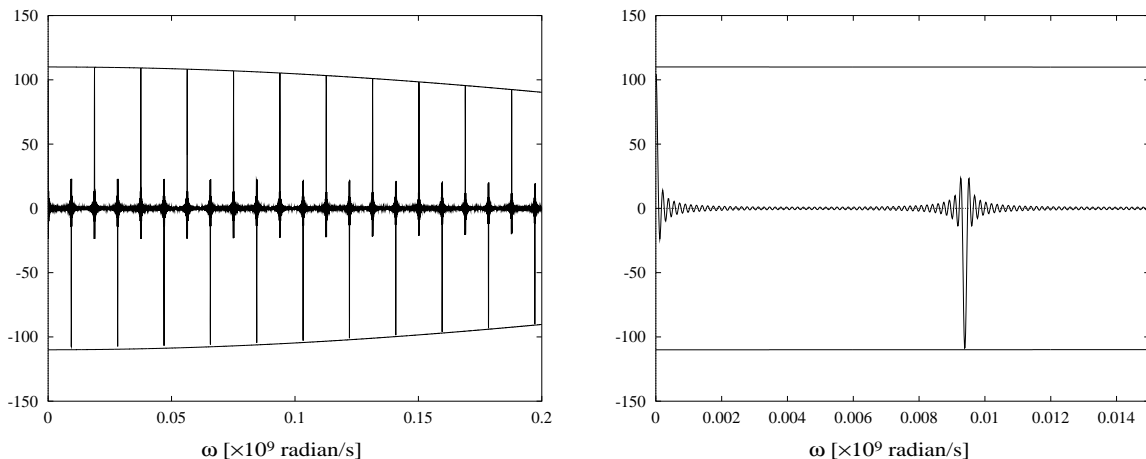
Figure. (6.3) Plot of the enhancement function times the envelope $\exp(-\sigma^2\omega^2/2)$ for $N_p = 120$, $N_b = 110$, $\tau_s = 12.7$ $\mu$s. The envelope function is plotted to guide the eye. The enlargement on the right shows the ripple caused by the gap of 10 missing bunches at a frequency of 78 kHz.

## 6.2 Momentum spread

So far we have assumed that the particles are all oscillating at the same frequency. In fact any real beam has a nonzero momentum spread, and unless we have an isochronous ring, there will be a spread in the revolution frequencies of the individual particles. In the case of beams bunched by rf cavities, there will be synchrotron oscillations with each individual particle having a varying revolution period.

### 6.2.3 Longitudinal Schottky spectrum of an unbunched beam

The current of the $m^{\text{th}}$ particle can be written as

$$i_m(t) = q f_m \sum_{n=-\infty}^{\infty} e^{jn[\omega_m t + \psi_m]}$$

$$= q f_m \left[ 1 + 2 \sum_{n=1}^{\infty} \cos[n(\omega_m t + \psi_m)] \right] \tag{6.10}$$

where $f_m = \omega_m/2\pi$ and $\psi_m$ are the respective revolution frequency and phase of the particle.

Averaging over $N$ particles in the beam the rms frequency spread of the $n^{\text{th}}$ revolution harmonic of the synchronous particle's frequency $f_s$ will be the absolute value of

$$\text{harmonic bandwidth} = n\sigma_f = n f_s \, |\eta_{\text{tr}}| \frac{\sigma_p}{p}, \tag{6.11}$$

where we recall that the phase slip factor was defined in Ref. [2] as

$$\eta_{\text{tr}} = \frac{1}{\gamma^2} - \frac{1}{\gamma_{\text{tr}}^2}. \tag{6.12}$$

The total average current for a large number of particles is

$$\langle i \rangle = \sum_{i=1}^{N} i_m(t) = Nq\langle f \rangle = Nq f_s, \tag{6.13}$$

which is just the dc component of the current. The rms component of current may be found from

$$
\begin{aligned}
\sigma_i^2 &= \left\langle (i - \langle i \rangle)^2 \right\rangle \\
&= \left\langle \left[ \sum_{m=1}^{N} q f_m \left( 1 + 2 \sum_{n=1}^{\infty} \cos(n\omega_m t + \psi_m) \right) - N q f_s \right]^2 \right\rangle \\
&= 2 q^2 f_s^2 N.
\end{aligned}
\tag{6.14}
$$

So the rms current component is then

$$
\sigma_i = q f_s \sqrt{2N},
\tag{6.15}
$$

which is independent of harmonic number. The bandwidth is however proportional to the number $n$ of the revolution harmonic as given by Eq. (6.11) and indicated in Fig. (6.4).
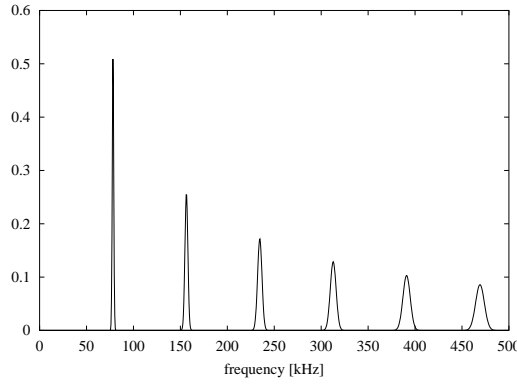


Figure. 6.4 Plot of first six revolution harmonics. (I have exaggerated the momentum spread so that the widths can be seen.) Note that the area under each peak (i.e., peak times width) is constant.

### 6.2.4 Synchrotron oscillations of a single particle

For simplicity, consider only a single particle which is now undergoing a small synchrotron oscillation. This modulates the arrival time at the detector as

$$
t \rightarrow t + a \sin(\Omega_s t + \psi),
\tag{6.16}
$$

where $a$ ($\ll \tau_s$) and $\psi$ are respectively the amplitude and phase of modulation. The current seen by the detector on the $n^{\text{th}}$-turn is then

$$
\begin{aligned}
i_n &= \sum_{n=-\infty}^{\infty} q \, \delta \left( t - n \left[ \tau_s + a \sin(\Omega_s n \tau_s + \psi) \right] \right) \\
&\simeq \frac{q}{\tau_s} \sum_{n=-\infty}^{\infty} e^{j n \omega_s [\tau_s + a \sin(n\Omega_s \tau_s + \psi)]},
\end{aligned}
\tag{6.17}
$$

where we have made use of the identity

$$
\sum_{-\infty}^{\infty} \delta(t - n\tau) = \frac{1}{\tau} \sum_{-\infty}^{\infty} e^{j \frac{n 2\pi t}{\tau}}.
\tag{6.18}
$$

Recalling another identity

$$e^{jz\sin\theta} = \sum_{m=-\infty}^{\infty} J_m(z)\,e^{j\theta}, \tag{6.19}$$

we may now write

$$i_n = q \sum_{n=-\infty}^{\infty} e^{-jn\omega_s\tau_s} \sum_{m=-\infty}^{\infty} J_m(n\omega_s a)\,e^{-jm(n\omega_s\tau_s+\psi)}. \tag{6.20}$$

Now each revolution harmonic gets split into a sequence of synchrotron satellites of relative height $J_m(a)$ for the $m^{\text{th}}$ satellite. Since $J_m(n\omega_s a)$ decreases with increasing $m$ only the nearest lines are important. As a rule of thumb, lines with $m \gtrsim n\,2a\omega_s$ are negligible[1].
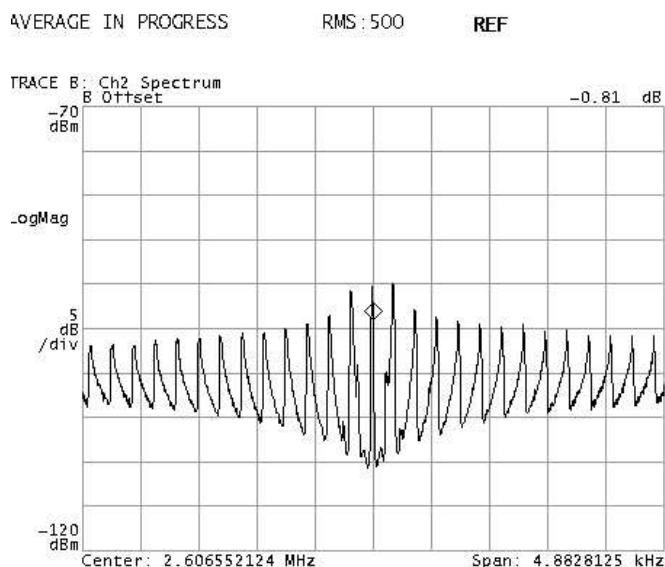


Figure. 6.5 Longitudinal spectrum showing synchrotron sidebands of a high order revolution line in RHIC. The pickup was a small Schottky cavity with a resonant frequency near 2 GHz. The signal was mixed down to the lower range of the spectrum analyzer. The peak in the middle is a revolution line of infinitesimal width, although the spike as measured does not go to infinity due to the finite bandwidth of the analyzer. The characteristic shape of the sidebands, as having a sharp edge away from the revolution line with a sloping fall towards the revolution line, is due to the fact that the synchrotron frequency is a maximum at the center of the bucket, where the particle distribution also peaks, and then falls off toward the edge of the bucket.

## 6.3 Transverse Schottky spectra

### 6.3.5 Transverse spectrum of an unbunched beam

Again we first consider a single particle with a betatron oscillation in one plane. Here we must use a transverse pickup which is sensitive to the amplitude $a_m$ of the oscillation. The measured signal is then proportional to the dipole oscillation signal

$$d_m = a_m(t)i_m(t), \tag{6.21}$$

for the $m^{\text{th}}$ particle. We immediately see that the signal is proportional to both the amplitude of oscillation and to the current of the bunch, so in addition to the effect of betatron oscillations, transverse spectra may also exhibit aspects of the longitudinal spectra. For the betatron oscillation we have

$$a_m(t) = a_m \cos(\text{q}_m \omega_m t + \psi_m), \tag{6.22}$$

where $\text{q}_m$ is the fractional part of the betatron tune, and $\omega_m/2\pi$ and $\psi_m$ are respectively the particle's revolution frequency and betatron-phase offset. Eq. (6.21) now becomes

$$
\begin{aligned}
d_m(t) &= a_m \cos(\text{q}_m \omega_m t + \psi_m)\, q f_m \sum_{n=-\infty}^{\infty} e^{jn\omega_m t} \\
&= \frac{q a_m f_m}{2} \left( e^{j(\text{q}_m \omega_m t + \psi_m)} + e^{-j(\text{q}_m \omega_m t + \psi_m)} \right) \sum_{n=-\infty}^{\infty} e^{jn\omega_m t} \\
&= \frac{q a_m f_m}{2} \sum_{n=-\infty}^{\infty} \left( e^{j[(n+\text{q}_m)\omega_m t + \psi_m]} + e^{j[(n-\text{q}_m)\omega_m t - \psi_m]} \right) \\
&= \frac{q a_m f_m}{2} \sum_{n=-\infty}^{\infty} \left( e^{j[(n+\text{q}_m)\omega_m t + \psi_m]} + e^{-j[(n+\text{q}_m)\omega_m t + \psi_m]} \right) \\
&= q a_m f_m \sum_{n=-\infty}^{\infty} \cos[(n+\text{q}_m)\omega_m t + \psi_m]. \tag{6.23}
\end{aligned}
$$

So the spectrum will have lines spaced like the revolution harmonics but offset by an amount $\text{q}_m f_m$. Since we cannot tell the difference between negative and positive frequencies, the negative frequencies fold over to give lines at $(n \pm \text{q}_m)f_m$ as shown in Fig. (6.6).
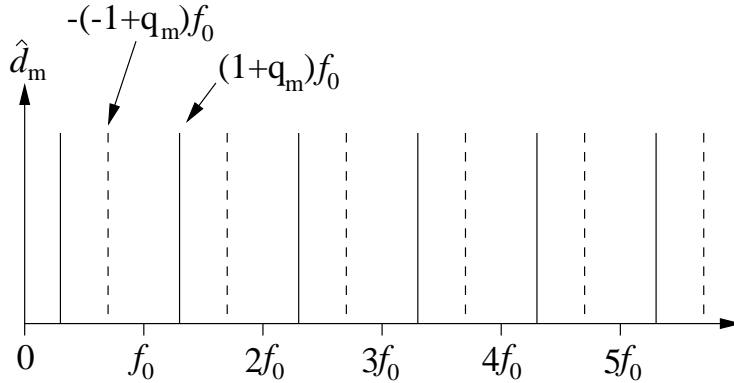


Figure. 6.7 Spectrum of betatron lines. The dashed lines are folded over from negative frequencies by plotting the absolute value $|(n + \text{q})f_s|$. Here I have plotted lines for $\text{q} < 0.5$.

Summing over $N$ particles we get the total average transverse signal

$$\langle d \rangle = 0, \tag{6.24}$$

with the rms spread

$$\sigma_d = \sqrt{\langle (d_m - \langle d_m \rangle)^2 \rangle} = q f_s\, \sigma_a \sqrt{\frac{N}{2}}, \tag{6.25}$$

where $\sigma_a$ is the rms betatron amplitude. The Schottky power in each sideband is proportional to $\sigma_d^2$ and is again independent of the revolution harmonic number $n$.

Comparing Eqs. (6.15 & 6.25) we see that the rms betatron amplitude may be obtained from

$$\sigma_a = \frac{2\sigma_d}{\sigma_i}. \tag{6.26}$$

If the detectors are very well calibrated, then this can be used to obtain the transverse emittance.

The momentum spread and betatron tune spread contribute to give a nonzero width to the betatron line. If the betatron tune spread is only due to chromaticity, then

$$\sigma_{\mathrm{q}} = |(n + \mathrm{q})\eta_{\mathrm{tr}} + Q\xi| \frac{\sigma_p}{p}, \tag{6.27}$$

where $Q$ is the total betatron tune (including integer part) and $\xi$ is the chromaticity

$$\xi = \frac{p}{Q} \frac{dQ}{dp}. \tag{6.28}$$

Other contributions to the betatron tune spread which are not chromatic should be added in quadrature with Eq. (6.27), since they would be independent of the momentum oscillation.

For large values of $n$, the fractional part of the tune becomes negligible and the width of the band is

$$\sigma_{\mathrm{q}} \simeq |n\eta_{\mathrm{tr}} + Q\xi| \frac{\sigma_p}{p}, \tag{6.29}$$

We now see that the widths of the upper and lower sidebands are different since $n$ can be either positive or negative. Whether the upper is narrower or wider depends on the signs of $\eta_{\mathrm{tr}}$, $n$, and $\xi$.

### 6.3.6 Transverse spectrum of a single bunch

As alluded to in the previous section, the transverse oscillation in Eq. (6.21) is modulated by the bunch current, so we should expect to see the additional structure of the longitudinal spectra superimposed on the betatron lines of the previous section.

Due to a lack of time, I will defer the development of this section to the future. There is probably more in this chapter than we will cover in class anyway. I recommend Boussard's article[1] for more information. I have added a few pictures of Schottky measurements from RHIC showing the betatron sidebands.
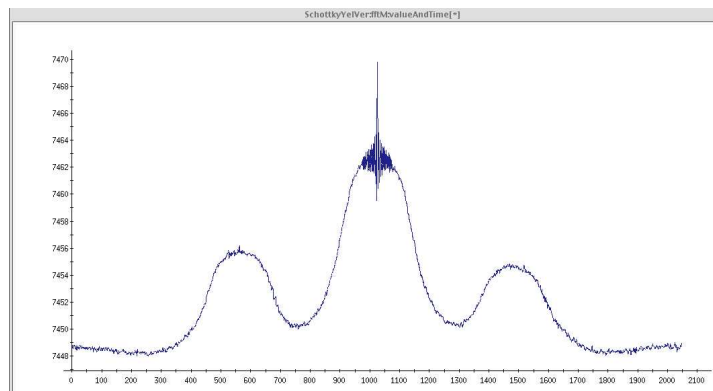


Figure. 6.8 Transverse Schottky spectrum from RHIC. The middle rounded bump is generated by the synchrotron sidebands which were not resolved by the bandwidth of the scope. The lower bumps to either side are the betatron sidebands. Unfortunately, the program used to plot this did not label the axes in physical units. The width of horizontal scale is about the revolution frequency, 78 kHz.
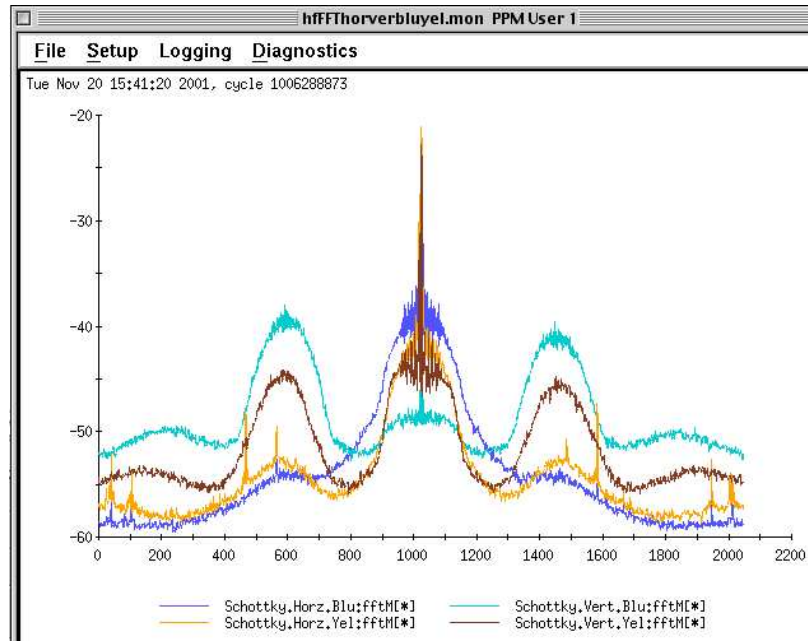
Figure. 6.9 Simultaneous Schottky signals measured for horizontal and vertical transverse motion in both the RHIC rings.
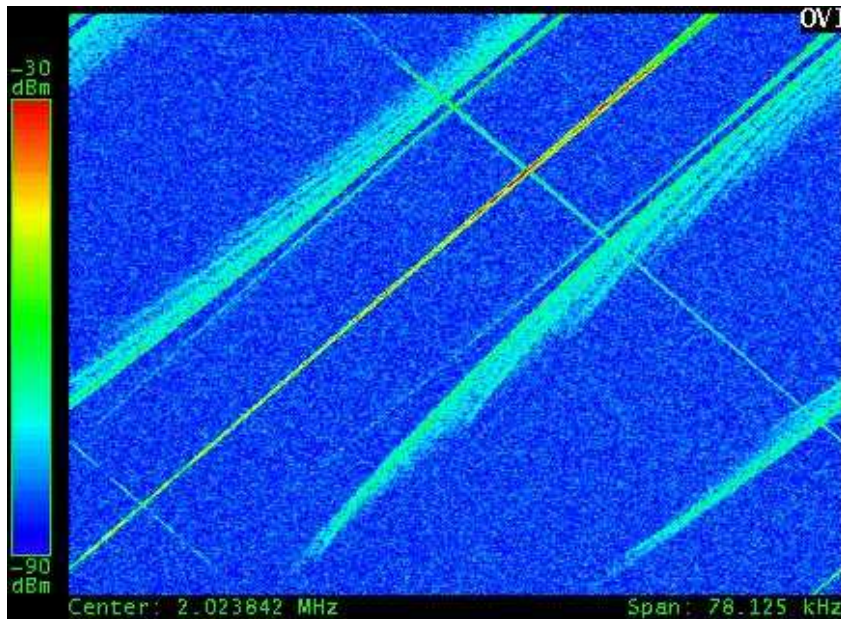


Figure. 6.10 Waterfall plot of transverse Schottky spectra of gold beam in RHIC during an energy ramp. Time increases from the top to the bottom, and individual Schottky spectra measurements are plotted horizontally. The thin straight line moving to the left (from upper right to lower left) is a revolution line. The next broad lines to either side are betatron sidebands. At the lower right there is just a hint of the next higher revolution line, with one of its corresponding betatron sideband lines. Notice how the betatron sidebands are filamenting as beam is slowly lost. The other two faint lines moving to the right are interference artifacts, probably from some signal leaking into the mixer.
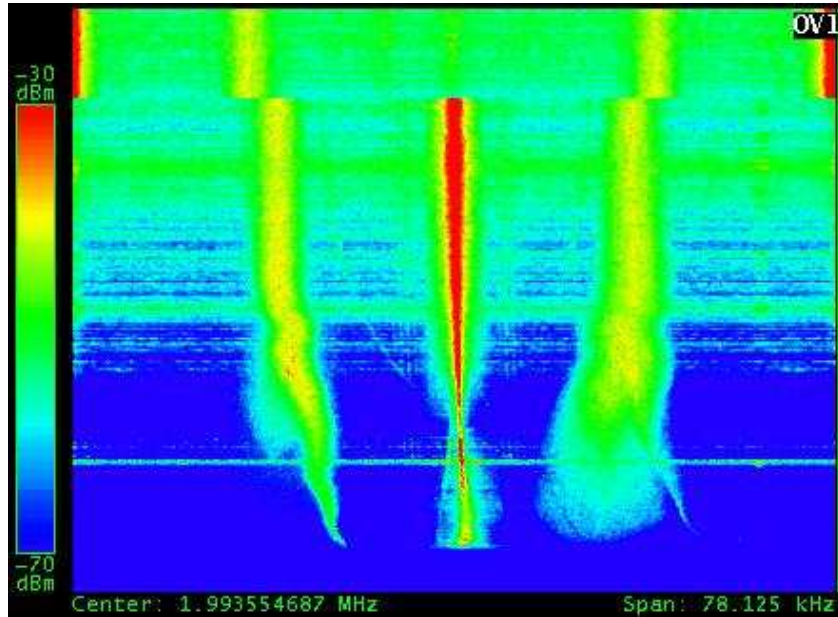
Figure. 6.11 Transverse Schottky waterfall plot during another ramp showing a revolution line in the center with two betatron sidebands. One can see that one sideband is broadening which indicates an increase in chromaticity. Again the beam was lost before the end of the ramp. (At the top you can see two revolution lines at the two edges. I'm not sure why the lines shift by half a revolution line spacing about a sixth of the way down. Presumably the reference frequency to the mixer jumped. I must investigate this. Perhaps it might be related to the phase jump at transition?) The horizontal lines (bands) in the top half show that there was a lot of broad spectrum power in the beam which is quite common, particularly before and just after transition.

### References for Chapter 6

[1] D. Boussard, "Schottky Noise and Beam Transfer Function Diagnostics", *CERN Accelerator School Fifth Advanced Accelerator Physics Course*, CERN 95-06, vol. II p749 (1993).

[2] M. Conte and W. W. MacKay, *An Introduction to the Physics of Particle Accelerators*, World Scientific, Singapore (1991).

# 7

# Leapfrog Integration of Equations of Motion

When we write simulation codes to integrate a system of equations of motion like

$$\frac{d\phi}{dt} = \alpha W \tag{7.1a}$$

$$\frac{dW}{dt} = -\beta\phi, \tag{7.1b}$$

where $\alpha$ and $\beta$ are constants, things sometimes go awry. An obvious way to solve this without computers is to write a second order differential equation:

$$\frac{d^2\phi}{dt^2} + \alpha\beta\,\phi = 0, \tag{7.2}$$

with solutions which are sine-like or exponential depending on the sign of $\alpha\beta$. For the case of $\omega^2 = \alpha\beta > 0$ we have

$$\phi(t) = \phi_0 \cos[\omega(t - t_0)],$$

which is periodic so that a particle traces out an ellipse in the $(\phi, W)$-phase space.

We frequently resort to integrating by stepping through a pair of difference equations. A simple naive approach may run into problems. First I will demonstrate the incorrect method with what might appear at first to be a reasonable choice of difference equations:

$$\phi_{n+1} = \phi_n + \alpha W_n\,\Delta t \tag{7.3a}$$

$$W_{n+1} = W_n - \beta\phi_n\Delta t, \tag{7.3b}$$

Writing them in matrix form we have

$$\begin{pmatrix} \phi_{n+1} \\ W_{n+1} \end{pmatrix} = \begin{pmatrix} 1 & \alpha\Delta t \\ -\beta\Delta t & 1 \end{pmatrix} \begin{pmatrix} \phi_n \\ W_n \end{pmatrix} = \mathbf{M} \begin{pmatrix} \phi_n \\ W_n \end{pmatrix}, \tag{7.4}$$

where the

$$\det(\mathbf{M}) = 1 + \alpha\beta\Delta t^2 \neq 1 \tag{7.5}$$

unless either $\alpha$ or $\beta$ are zero. For $\omega^2 = \alpha\beta > 0$ this would give results with the particle proceeding to larger amplitudes in phase space instead of tracing out an ellipse. The resulting integration is nonsymplectic.
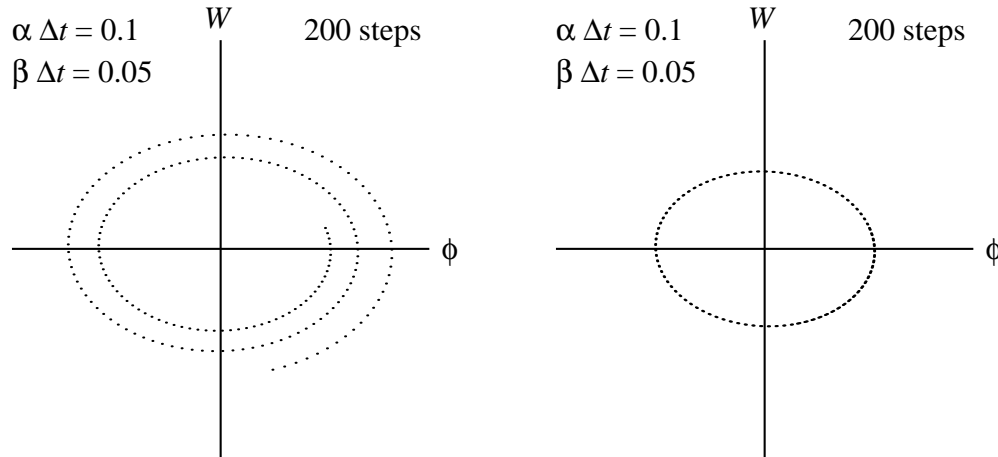
30

Figure. (7.1) The plot on the left shows how the improper method causes a blowup of the oscillation, whereas the plot on the right was tracked with the leap-frog method.

$$\phi_{\frac{1}{2}} \longrightarrow \phi_{1+\frac{1}{2}} \longrightarrow \phi_{2+\frac{1}{2}}$$
$$W_1 \longrightarrow W_2 \longrightarrow W_3$$

Figure. 7.2 By integrating the variables so that the time steps hop over each other, we can obtain a symplectic result.

If instead we consider Eqs. (7.1) as modeling the longitudinal motion in a circular ring with a single rf cavity, then a convenient time step would correspond to one turn with a long drift followed by a small thin-lens-type energy kick:

$$
\begin{pmatrix} \phi_{n+\frac{1}{2}} \\ W_{n+1} \end{pmatrix} = \begin{pmatrix} 1 & 0 \\ -\beta\Delta t & 1 \end{pmatrix} \begin{pmatrix} 1 & \alpha\Delta t \\ 0 & 1 \end{pmatrix} \begin{pmatrix} \phi_{n-\frac{1}{2}} \\ W_n \end{pmatrix}
$$
$$
= \begin{pmatrix} 1 & \alpha\Delta t \\ -\beta\Delta t & 1 - \alpha\beta\Delta t \end{pmatrix} \begin{pmatrix} \phi_{n-\frac{1}{2}} \\ W_n \end{pmatrix}
$$
$$
= \mathbf{M} \begin{pmatrix} \phi_{n-\frac{1}{2}} \\ W_n \end{pmatrix},
$$

with

$$\det(M) = 1. \tag{7.7}$$

This type of two-step integration where one variable is integrated ($\phi_{n-\frac{1}{2}} \to \phi_{n+\frac{1}{2}}$) and then the other is integrated ($W_n \to W_{n+1}$) is referred to as *leap-frog* integration, since the time steps for the two variables are interleaved as indicated by Fig. (7.2).

References for Chapter 7

[1] R. W. Hockney and J. W. Eastwood, *Computer Simulation Using Particles*, Adam Hilger, Bristol (1988).

# 8

# Example of Coupled Bunch Instability

During one ramp of polarized protons in Yellow ring of RHIC, only one of the two 28 MHz cavities for acceleration was being powered. The tuner for the other cavity was detuned to a fixed frequency away from the proper frequency. As the beam was accelerated from 24.3 GeV at injection to 100 GeV at storage the revolution frequency shifts from $f_{\mathrm{rf},i} = 28.1297$ MHz to $f_{\mathrm{rf},f} = 28.1494$ MHz. The normal harmonic number for the 28 MHz cavities is $h = 360$. At one point in the ramp, the $358^{\mathrm{th}}$ harmonic of the revolution frequency crossed the resonant frequency of the unpowered cavity initiating the multibunch instability shown in Fig. (8.1).
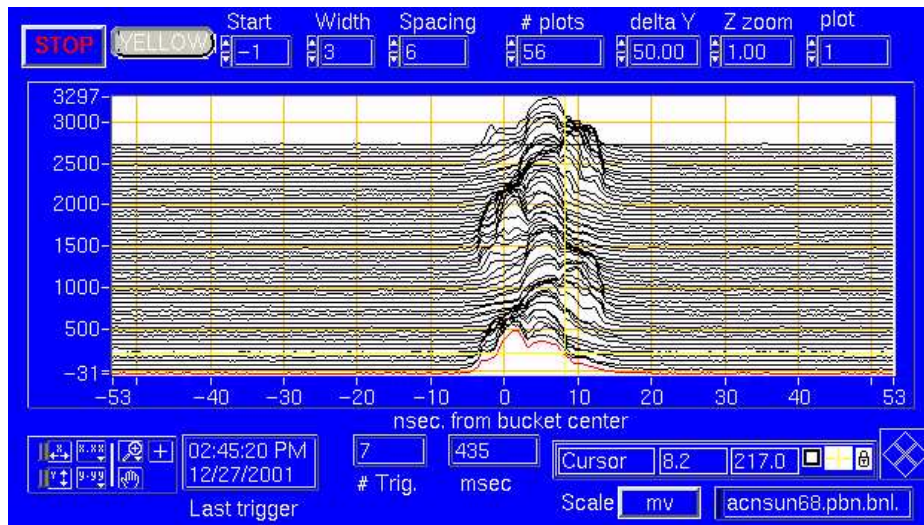


Figure. 8.1 Coupled bunch instability in the RHIC Yellow ring during acceleration of polarized protons. The 56 traces are the 55 bunches (plus one empty bucket) taken on one turn during acceleration. The populate every sixth rf bucket starting from bucket 1 up to bucket 331. There is a gap of 5 bunches (buckets 332-360) to leave room for the rise time of the abort kickers.

The bunched beam drives $TM_{010}$ oscillations in the unpowered cavity. Each bunch will see the wake of previous bunches and gain (loose) a little energy from (to) the cavity depending on the relative phase of the wake oscillation when the bunch crosses the gap. As a result there is a slight beating of frequencies of the two cavities as indicated in Fig. (8.2).
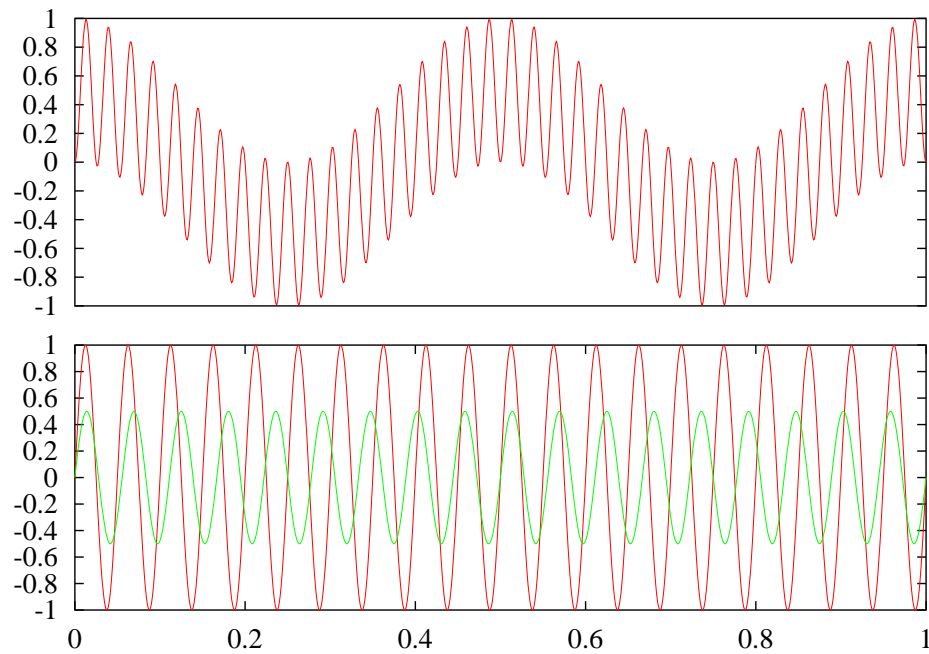
Figure. 8.2 Conceptual beating of the frequencies of the two cavities: $[\sin(2\pi hx)\sin(2\pi h'x)]$. Here the harmonic numbers $h = 20$ $[\sin(2\pi hx)]$ and $h' = 18$ $[0.5\sin(2\pi h'x)]$ were used rather than 360 and 358, so that the individual cycles could be seen for the individual cavities.
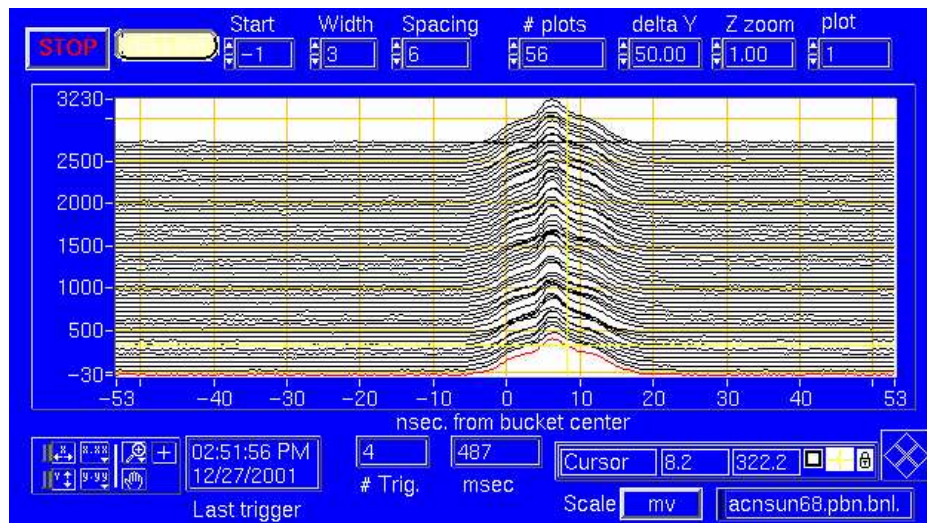


Figure. 8.3  This shows the 55 bunches later in the acceleration ramp after the oscillations have Landau damped.

# 9

# Luminosity as Calculated from Machine Parameters

## 9.1 Introduction

The luminosity rate of interactions, at time $t$, between two colliding beams may be easily understood by treating one beam as a target, with number density $\rho_2(\vec{\mathbf{X}}_2, t)$, and the other as an incident beam, whose flux density is $v\rho_1(\vec{\mathbf{X}}_1, t)$, where

$$v = |\vec{v}_1 - \vec{v}_2| \tag{9.1}$$

is the relative velocity.† The coordinates $\mathbf{X}_2$ and $\mathbf{X}_1$ are points in the six dimensional phase space $(x, x', y, y', s, \delta)$. The interaction rate may then be written as

$$\frac{dN}{dt} = \int \sigma(\vec{\mathbf{X}}_2, \vec{\mathbf{X}}_1)\, \rho_2(\vec{\mathbf{X}}_2, t)\, |\vec{v}_1 - \vec{v}_2|\, \rho_1(\vec{\mathbf{X}}_1, t)\, d^6\mathbf{X}_2\, d^6\mathbf{X}_1, \tag{9.2}$$

where $\sigma$ is the cross section for single particle interactions.

Of course, for the actual rate seen by an experiment one must fold in the detector acceptance and efficiency for a desired reaction by integrating the differential cross section times acceptance and efficiency over the the phase space of final particles.

For most high energy collisions the probability of interaction is extremely small, unless the particles are very close, e. g.,

$$|\vec{x}_1 - \vec{x}_2| \lesssim 10^{-15}\text{m}. \tag{9.3}$$

This is much less than the size of a typical beam ($\gtrsim 10^{-6}$m). It is therefore reasonable to approximate the cross section by

$$\sigma(\vec{\mathbf{X}}_2, \vec{\mathbf{X}}_1) \simeq \sigma(\vec{p}_2, \vec{p}_1)\, \delta^3(\vec{x}_1 - \vec{x}_2). \tag{9.4}$$

If the beams are almost monoenergetic, $\sigma$ may be factored outside the integral and replaced by the total cross section, so that

$$\frac{dN}{dt} \simeq |\vec{v}_1 - \vec{v}_2|\, \sigma(\vec{p}_2, \vec{p}_1) \int \rho_2(\vec{x}, t)\, \rho_1(\vec{x}, t)\, d^3x. \tag{9.5}$$

If the bunch shape does not change appreciably while the opposing bunches overlap, then the time dependence of the $i^{\text{th}}$ densities may be written as

$$\rho_i(\vec{x}, t) = \rho_i(\vec{x} - \vec{v}_i t),$$

---

† For relativistic colliding beams this relative velocity is the difference of the two velocities $v \simeq |c - (-c)| = 2c$ as calculated in the between the two beams. Perhaps the best way to think of this is that an observer in the rest system of the collision point sees the bunches pass through each other at twice the effective speed as a single bunch.

and the total number of interactions from one bunch crossing is

$$N = |\vec{v}_1 - \vec{v}_2|\,\sigma \int \rho_2(\vec{x} - \vec{v}_2 t)\,\rho_1(\vec{x} - \vec{v}_1 t)\,d^3x\,dt. \tag{9.6}$$

When there are $N_b$ equally spaced bunches per beam in a circular collider whose revolution frequency is $f_0$, the interaction rate per interaction region is

$$\frac{dN}{dt} = |\vec{v}_1 - \vec{v}_2|\,f_0 N_b \sigma \int \rho_2(\vec{x} - \vec{v}_2 t)\,\rho_1(\vec{x} - \vec{v}_1 t)\,d^3x\,dt. \tag{9.7}$$

The ratio of interaction rate to total cross section is called the instantaneous luminosity

$$\mathcal{L} = |\vec{v}_1 - \vec{v}_2|\,f_0 N_b \int \rho_2(\vec{x} - \vec{v}_2 t)\,\rho_1(\vec{x} - \vec{v}_1 t)\,d^3x\,dt, \tag{9.8}$$

which for high energy collisions in the center of mass system becomes

$$\mathcal{L} = 2c f_0 N_b \int \rho_2(x, y, z - ct)\,\rho_1(x, y, z + ct)\,d^3x\,dt, \tag{9.9}$$

where beam-2 moves in the $+z$ direction. The total or integrated luminosity refers to the instantaneous luminosity integrated over the time of the experiment.

If the bunch densities change shape in the overlap region, then the simplification of Eq. 9.5 is invalid and the luminosity must be calculated from

$$\mathcal{L} = 2c f_0 N_b \int \rho_2(x, y, z, t)\,\rho_1(x, y, z, t)\,d^3x\,dt. \tag{9.10}$$

If the beams cross where the transverse beta-functions both have minima, then the minima of the beta-functions should not be smaller than the bunch length, otherwise too much of the overlap region has a lower density, and the peak luminosity is degraded. The beta-function about an interaction point goes like

$$\beta(s) = \beta^\star + \frac{s^2}{\beta^*}, \tag{9.11}$$

with the minimum value of $\beta^*$ at the interaction point $(s = 0)$. For bunches of length $l_b$, the overlap occurs between $s = \pm l_b/2$. If $l_b = \beta^\star$ the longitudinal centers of the bunches cross at $s = 0$ where $\beta = \beta^\star$ and the opposite ends of the bunches cross where $\beta = 1.25\beta^\star$.

## 9.2 Gaussian beam distributions

For one transverse horizontal degree of freedom the Courant-Snyder invariant is

$$\begin{aligned}
W_x &= (\,x_\beta \quad x'_\beta\,) \begin{pmatrix} \gamma_x & \alpha_x \\ \alpha_x & \beta_x \end{pmatrix} \begin{pmatrix} x_\beta \\ x'_\beta \end{pmatrix} \\
&= \gamma x_\beta^2 + 2\alpha x_\beta x'_\beta + \beta x'^2_\beta,
\end{aligned} \tag{9.12}$$

where $\beta_x$, $\alpha_x$, and $\gamma_x = (1 + \alpha_x^2)/\beta_x$ are the Twiss parameters for betatron motion, and $x_\beta$ and $x'_\beta$ are the transverse betatron coordinate and angle in a paraxial phase space. A Gaussian distribution of particles undergoing betatron oscillations for this degree of freedom may be written as

$$f_\beta(x_\beta, x'_\beta) = \frac{N_z}{2\pi\epsilon}e^{-\frac{1}{2}W_x/\epsilon_x}, \tag{9.13}$$

where $N$ is the number of particles and $\pi\epsilon_x$ is the rms horizontal emittance.

Similarly for the longitudinal motion we may write an invariant

$$
\begin{aligned}
W_z &= ( z \quad \delta ) \begin{pmatrix} \gamma_z & \alpha_z \\ \alpha_z & \beta_z \end{pmatrix} \begin{pmatrix} z \\ \delta \end{pmatrix} \\
&= \gamma_z z^2 + 2\alpha_z z\delta + \beta_z \delta^2,
\end{aligned}
\tag{9.14}
$$

The corresponding longitudinal distribution function for a Gaussian bunch is

$$
f_z(z,\delta) = \frac{N}{2\pi\epsilon_z} e^{-\frac{1}{2}W_z/\epsilon_z},
\tag{9.15}
$$

where $z = s - vt$ and $\delta = \Delta p/p$ are respectively the longitudinal and fractional momentum deviations of a particle from the design particle when it passes the coordinate $s$.

The total transverse coordinates are the sum of the betatron coordinates and the effect of dispersion:

$$
X = \begin{pmatrix} x \\ x' \end{pmatrix} = \begin{pmatrix} x_\beta \\ x'_\beta \end{pmatrix} + \begin{pmatrix} 0 & \eta_x \\ 0 & \eta'_x \end{pmatrix} \begin{pmatrix} z \\ \delta \end{pmatrix},
\tag{9.16}
$$

where $\eta_x$ and $\eta'_x$ are the horizontal closed-orbit dispersion functions. Since the Jacobian of the transformation from coordinates $(x_\beta, x'_\beta, z, \delta)$ to $(x, x', z, \delta)$ is one, we may write a combined distribution function as

$$
f(x, x', z, \delta) = \frac{N}{(2\pi)^2 \epsilon_x \epsilon_z} e^{-\frac{1}{2}[(X-DZ)^\mathrm{T}\Xi_\beta(X-DZ)+Z^\mathrm{T}\Xi_z Z]},
\tag{9.17}
$$

with the definitions:

$$
X = \begin{pmatrix} x \\ x' \end{pmatrix}, \quad Z = \begin{pmatrix} z \\ \delta \end{pmatrix}, \quad D = \begin{pmatrix} 0 & \eta_x \\ 0 & \eta'_x \end{pmatrix},
\tag{9.18}
$$

$$
\Xi_\beta = \frac{1}{\epsilon_x} \begin{pmatrix} \gamma_x & \alpha_x \\ \alpha_x & \beta_x \end{pmatrix}, \quad \text{and} \quad \Xi_z = \frac{1}{\epsilon_z} \begin{pmatrix} \gamma_z & \alpha_z \\ \alpha_z & \beta_z \end{pmatrix}.
\tag{9.19}
$$

Rearranging terms in the distribution and adding in a similar distribution function for uncoupled vertical betatron motion yields the equation

$$
f(x, x', y, y', z, \delta) = \frac{N}{(2\pi)^3 \epsilon_x \epsilon_y \epsilon_z} e^{-\frac{1}{2}\hat{X}^\mathrm{T}\Xi\hat{X}},
\tag{9.20}
$$

where

$$
\hat{X} = \begin{pmatrix} x \\ x' \\ y \\ y' \\ z \\ \delta \end{pmatrix}, \quad \text{and}
\tag{9.21}
$$

$$
\Xi = \begin{pmatrix}
\frac{\gamma_x}{\epsilon_x} & \frac{\alpha_x}{\epsilon_x} & 0 & 0 & 0 & -\frac{\gamma_x \eta_x + \alpha_x \eta'_x}{\epsilon_x} \\
\frac{\alpha_x}{\epsilon_x} & \frac{\beta_x}{\epsilon_x} & 0 & 0 & 0 & -\frac{\alpha_x \eta_x + \beta_x \eta'_x}{\epsilon_x} \\
0 & 0 & \frac{\gamma_y}{\epsilon_y} & \frac{\alpha_y}{\epsilon_y} & 0 & 0 \\
0 & 0 & \frac{\alpha_y}{\epsilon_y} & \frac{\beta_y}{\epsilon_y} & 0 & 0 \\
0 & 0 & 0 & 0 & \frac{\gamma_z}{\epsilon_z} & \frac{\alpha_z}{\epsilon_z} \\
-\frac{\gamma_x \eta_x + \alpha_x \eta'_x}{\epsilon_x} & -\frac{\alpha_x \eta_x + \beta_x \eta'_x}{\epsilon_x} & 0 & 0 & \frac{\alpha_z}{\epsilon_z} & \frac{\beta_z}{\epsilon_z} + \frac{H}{\epsilon_x}
\end{pmatrix},
\tag{9.22}
$$

with the function $H = \gamma_x \eta_x^2 + 2\alpha_x \eta_x \eta_x' + \beta_x \eta_x'^2$. The function $H$ is sometimes mistakenly called the *dispersion invariant* since it is constant through regions of the lattice with no bends (i. e., straight sections). It is however **not** an invariant inside bends and will in general be different from one bend free region to the next. With a bit of algebra one can show that

$$\det(\Xi) = \frac{1}{\epsilon_x^2 \epsilon_y^2 \epsilon_z^2}. \tag{9.23}$$

The beam sigma matrix ($\Sigma$) or variance matrix for the distribution is just the inverse of $\Xi$:

$$\Sigma = \begin{pmatrix} \beta_x \epsilon_x + \eta_x^2 \sigma_\delta^2 & -\alpha_x \epsilon_x + \eta_x \eta_x' \sigma_\delta^2 & 0 & 0 & -\eta_x \alpha_z \epsilon_z & \eta_x \sigma_\delta^2 \\ -\alpha_x \epsilon_x + \eta_x \eta_x' \sigma_\delta^2 & \gamma_x \epsilon_x + \eta_x'^2 \sigma_\delta^2 & 0 & 0 & -\eta_x' \alpha_z \epsilon_z & \eta_x' \sigma_\delta^2 \\ 0 & 0 & \beta_y \epsilon_y & -\alpha_y \epsilon_y & 0 & 0 \\ 0 & 0 & -\alpha_y \epsilon_y & \gamma_y \epsilon_y & 0 & 0 \\ -\eta_x \alpha_z \epsilon_z & -\eta_x' \alpha_z \epsilon_z & 0 & 0 & \beta_z \epsilon_z & -\alpha_z \epsilon_z \\ \eta_x \sigma_\delta^2 & \eta_x' \sigma_\delta^2 & 0 & 0 & -\alpha_z \epsilon_z & \sigma_\delta^2 \end{pmatrix}, \tag{9.24}$$

where $\sigma_\delta^2 = \gamma_z \epsilon_z$. Moreover if we consider coupling in all three dimensions, the beam sigma matrix may be written as the usual symmetric variance matrix for a Gaussian distribution:

$$\Sigma = \begin{pmatrix} \sigma_x^2 & \sigma_{xx'} & \sigma_{xy} & \sigma_{xy'} & \sigma_{xz} & \sigma_{x\delta} \\ \sigma_{xx'} & \sigma_{x'}^2 & \sigma_{x'y} & \sigma_{x'y'} & \sigma_{x'z} & \sigma_{x'\delta} \\ \sigma_{xy} & \sigma_{x'y} & \sigma_y^2 & \sigma_{yy'} & \sigma_{yz} & \sigma_{y\delta} \\ \sigma_{xy'} & \sigma_{x'y'} & \sigma_{yy'} & \sigma_{y'}^2 & \sigma_{y'z} & \sigma_{y'\delta} \\ \sigma_{xz} & \sigma_{x'z} & \sigma_{yz} & \sigma_{y'z} & \sigma_z^2 & \sigma_{z\delta} \\ \sigma_{x\delta} & \sigma_{x'\delta} & \sigma_{y\delta} & \sigma_{y'\delta} & \sigma_{z\delta} & \sigma_\delta^2 \end{pmatrix}, \tag{9.25}$$

which has 21 free parameters. The general Gaussian distribution is then given by

$$f(x, x', y, y', z, \delta) = \frac{N\sqrt{|\Xi|}}{(2\pi)^3} e^{-\frac{1}{2}\hat{X}^T \Xi \hat{X}}, \tag{9.26}$$

where $\Xi = \Sigma^{-1}$.

The distribution given by Eq. 9.26 has a simple hyperelliptical shape. For a long beam passing through minimum of the beta-function, it should have a dog-bone shape. So far we have described the particle distribution relative to a longitudinal position $s$, where the $z$ coordinate is a time-like coordinate specifying how far the particle in question is in advance of the design particle. In order to evaluate the overlap integral of two colliding beams, we need to specify the density function in terms of $(x, x', y, y', s, \delta; t)$, rather than $(x, x', y, y', z, \delta; s)$. For a particle of velocity $v$, the relation between $s$, $z$, and $t$ is $z = vt - s$, and the required transformation between coordinates is defined by

$$\hat{X}(x, x', y, y', z, \delta; t) = M^{-1}\, \mathbf{X}(x, x', y, y', s, \delta; t), \tag{9.27}$$

i. e.,

$$\begin{pmatrix} x \\ x' \\ y \\ y' \\ z \\ \delta \end{pmatrix} = \begin{pmatrix} 1 & -s & 0 & 0 & 0 & 0 \\ 0 & 1 & 0 & 0 & 0 & 0 \\ 0 & 0 & 1 & -s & 0 & 0 \\ 0 & 0 & 0 & 1 & 0 & 0 \\ 0 & 0 & 0 & 0 & 1 & -\frac{\beta s}{\gamma^2} \\ 0 & 0 & 0 & 0 & 0 & 1 \end{pmatrix} \begin{pmatrix} x \\ x' \\ y \\ y' \\ vt - s \\ \delta \end{pmatrix} = \begin{pmatrix} x - x's \\ x' \\ y - y's \\ y' \\ vt - \left(1 + \frac{\beta\delta}{\gamma^2}\right)s \\ \delta \end{pmatrix} \tag{9.28}$$

where $\beta = v/c$ and $\gamma = \sqrt{1-\beta^2}$ are the usual Lorentz parameters. Substituting Eq. 9.28 into Eq. 9.26 gives

$$f(x, x', y, y', s, \delta; t) = \frac{N\sqrt{|\Xi|}}{(2\pi)^3} e^{-\frac{1}{2}\mathbf{X}^{\mathrm{T}}(\mathrm{M}^{-1})^{\mathrm{T}}\Xi\mathrm{M}^{-1}\mathbf{X}}, \tag{9.29}$$

which will now have the correct dog-bone shape at the waist. For high energy bunched beams the $\frac{\beta\delta}{\gamma^2} \ll 1$ and may be ignored. (For RHIC $\frac{\beta\delta}{\gamma^2} \lesssim 10^{-7}$.) Integrating Eq. 9.29 over the momentum-like coordinates yields the particle density per volume as a function of spatial coordinate and time:

$$\rho(x, y, s; t) = \frac{N\sqrt{|\Xi|}}{(2\pi)^3} \iiint e^{-\frac{1}{2}\mathbf{X}^{\mathrm{T}}(\mathrm{M}^{-1})^{\mathrm{T}}\Xi\mathrm{M}^{-1}\mathbf{X}} \, dx' \, dy' \, d\delta. \tag{9.30}$$

Let us now consider the limited case of a crossing point located in a straight section with no dispersion or horizontal-vertical coupling; here $\Xi$ of Eq. 9.22 becomes block-diagonal:

$$\Xi = \begin{pmatrix} \frac{\gamma_x}{\epsilon_x} & \frac{\alpha_x}{\epsilon_x} & 0 & 0 & 0 & 0 \\ \frac{\alpha_x}{\epsilon_x} & \frac{\beta_x}{\epsilon_x} & 0 & 0 & 0 & 0 \\ 0 & 0 & \frac{\gamma_y}{\epsilon_y} & \frac{\alpha_y}{\epsilon_y} & 0 & 0 \\ 0 & 0 & \frac{\alpha_y}{\epsilon_y} & \frac{\beta_y}{\epsilon_y} & 0 & 0 \\ 0 & 0 & 0 & 0 & \frac{\gamma_z}{\epsilon_z} & \frac{\alpha_z}{\epsilon_z} \\ 0 & 0 & 0 & 0 & \frac{\alpha_z}{\epsilon_z} & \frac{\beta_z}{\epsilon_z} \end{pmatrix}. \tag{9.31}$$

With this form, the integration of Eq. 9.30 is fairly simple and gives:

$$\rho(x, y, s; t) = \frac{Ne^{-\frac{x^2}{2\epsilon_x(\beta_x^* - 2\alpha_x^* s + \gamma_x^* s^2)}} e^{-\frac{y^2}{2\epsilon_y(\beta_y^* - 2\alpha_y^* s + \gamma_y^* s^2)}} e^{-\frac{(vt-s)^2}{2\epsilon_z\beta_z^*}}}{\sqrt{(2\pi)^3(\beta_x^* - 2\alpha_x^* s + \gamma_x^* s^2)(\beta_y^* - 2\alpha_y^* s + \gamma_y^* s^2)\beta_z^*\epsilon_x\epsilon_y\epsilon_z}}, \tag{9.32}$$

where the superscript "$*$"'s refer to the value at the design crossing point where $s = 0$. It is worthwhile noting that the expressions of transverse Twiss parameters in parentheses are just the evolution of the transverse $\beta$-functions along $s$:

$$\beta_x(s) = \beta_x^* - 2\alpha_x^* s + \gamma_x^* s^2, \qquad \text{and} \qquad \beta_y(s) = \beta_y^* - 2\alpha_y^* s + \gamma_y^* s^2. \tag{9.33}$$

For two colliding bunches the densities may be written as

$$\rho_1(x, y, s; t) = \frac{N_1 e^{-\frac{x^2}{2\epsilon_{x1}\beta_{x1}(s)}} e^{-\frac{y^2}{2\epsilon_{y1}\beta_{y1}(s)}} e^{-\frac{(s-vt)^2}{2\epsilon_{z1}\beta_{z1}^*}}}{\sqrt{(2\pi)^3\epsilon_{x1}\epsilon_{y1}\epsilon_{z1}\beta_{x1}(s)\beta_{y1}(s)\beta_{z1}^*}}, \tag{9.34}$$

with the $s$-axis taken along the trajectory of beam-1 and

$$\rho_2(x, y, s; t) = \frac{N_2 e^{-\frac{(x-h_x-\theta_x s)^2}{2\epsilon_{x2}\beta_{x2}(s)}} e^{-\frac{(y-h_y-\theta_y s)^2}{2\epsilon_{y2}\beta_{y2}(s)}} e^{-\frac{(s+vt+\Delta)^2}{2\epsilon_{z2}\beta_{z2}^*}}}{\sqrt{(2\pi)^3\epsilon_{x2}\epsilon_{y2}\epsilon_{z2}\beta_{x2}(s)\beta_{y2}(s)\beta_{z2}^*}}, \tag{9.35}$$
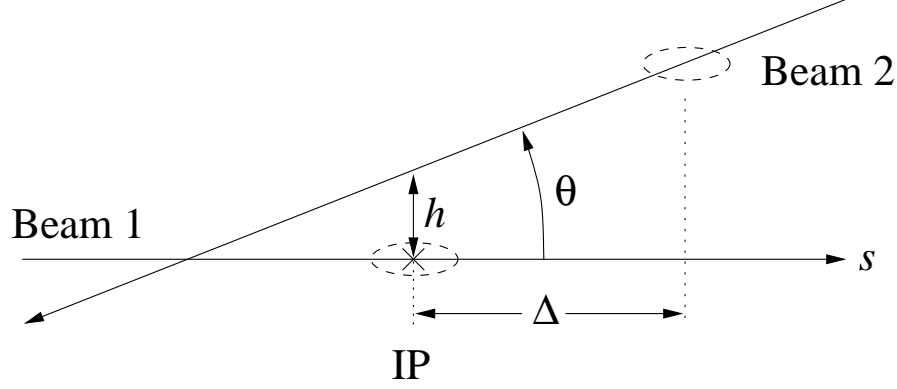
Figure. 9.1 Geometry of errors at the beam's crossing point.

the trajectory of beam-2 being offset at $s = 0$ by $h_x$ in the $x$-direction and $h_y$ in the $y$-direction. (See Fig. 9.1.) Using a small angle approximation, the slopes of the second beam's trajectory in the $x$ and $y$ directions are respectively $\theta_x$ and $\theta_y$ relative to the first beam's trajectory. The parameter $\Delta$ accounts for a mistiming of the bunch crossing; the bunches then cross at $s = \Delta/2$ from the design interaction point. The luminosity of this bunch crossing may be found by integrating the overlap of the two densities:

$$L = 2v \iiiint \rho_1(x, y, s; t)\rho_2(x, y, s; t)\, dx\, dy\, ds\, dt. \tag{9.36}$$

Integrating the $x$-dependent exponentials over $x$ yields

$$\int_{-\infty}^{\infty} e^{-\frac{(x - h_x - \theta_x s)^2}{2\epsilon_{x1}\beta_{x1}(s)}} e^{-\frac{x^2}{2\epsilon_{x2}\beta_{x2}(s)}}\, dx = \sqrt{\frac{2\pi\epsilon_{x1}\epsilon_{x2}\beta_{x1}(s)\beta_{x2}(s)}{\epsilon_{x1}\beta_{x1}(s) + \epsilon_{x2}\beta_{x2}(s)}}\, e^{-\frac{(h_x + \theta_x s)^2}{2[\epsilon_{x1}\beta_{x1}(s) + \epsilon_{x2}\beta_{x2}(s)]}}. \tag{9.37}$$

A similar integral occurs for the $y$-dimension. The integral of the $t$-dependent exponentials is

$$\int_{-\infty}^{\infty} e^{-\frac{(s - vt)^2}{2\epsilon_{z1}\beta_{z1}^*}} e^{-\frac{(s + vt + \Delta)^2}{2\epsilon_{z2}\beta_{z2}^*}}\, v\, dt = \sqrt{\frac{2\pi\epsilon_{z1}\epsilon_{z2}\beta_{z1}^*\beta_{z2}^*}{\epsilon_{z1}\beta_{z1}^* + \epsilon_{z2}\beta_{z2}^*}}\, e^{-\frac{(2s + \Delta)^2}{2(\epsilon_{z1}\beta_{z1}^* + \epsilon_{z2}\beta_{z2}^*)}}. \tag{9.38}$$

Using these results Eq. 9.36 becomes

$$L = \int_{-\infty}^{\infty} \frac{2N_1 N_2\, e^{-\frac{(h_x + \theta_x s)^2}{2[\epsilon_{x1}\beta_{x1}(s) + \epsilon_{x2}\beta_{x2}(s)]}} e^{-\frac{(h_y + \theta_y s)^2}{2[\epsilon_{y1}\beta_{y1}(s) + \epsilon_{y2}\beta_{y2}(s)]}} e^{-\frac{(2s + \Delta)^2}{2(\epsilon_{z1}\beta_{z1}^* + \epsilon_{z2}\beta_{z2}^*)}}}{\sqrt{(2\pi)^3 [\epsilon_{x1}\beta_{x1}(s) + \epsilon_{x2}\beta_{x2}(s)][\epsilon_{y1}\beta_{y1}(s) + \epsilon_{y2}\beta_{y2}(s)][\epsilon_{z1}\beta_{z1}^* + \epsilon_{z2}\beta_{z2}^*]}}\, ds, \tag{9.39}$$

for a single crossing of two bunches.

For the special case where the colliding beams are collinear with identical beam sizes and shapes at the interaction point, and having $2\sigma_z \lesssim \beta_x^*$, $2\sigma_z \lesssim \beta_y^*$, and $\Delta = 0$, the previous integral simplifies to

$$L = \frac{N_1 N_2}{4\pi\sigma_x\sigma_y}. \tag{9.40}$$

The average instantaneous luminosity for $N_b$ crossing bunches per revolution with $N_1$ and $N_2$ particles per bunch respectively for the opposing beams is then

$$\mathcal{L} = \frac{f_0 N_b N_1 N_2}{4\pi\sigma_x\sigma_y}. \tag{9.41}$$

When the beams are round with $\epsilon_{\rm rms} = \epsilon_x^{\rm rms} = \epsilon_y^{\rm rms}$ and $\beta^* = \beta_x^* = \beta_y^*$ and of equal current, then

$$\mathcal{L} = \frac{f_0 N_b N^2 \gamma}{4\pi\beta^*\epsilon_{\rm rms}}. \tag{9.42}$$

In a more realistic situation the different bunches may have random intensities, so that the product $N_b N_1 N_2$ must be replaced by a sum of the products of the colliding bunches' intensities, i. e.,

$$N_b N_1 N_2 \rightarrow \Sigma_{j=1}^{N_b} N_{1j} N_{2j}. \tag{9.43}$$

## 9.3 Estimation of luminosities in RHIC

Table I lists the RHIC design parameters for both protons and gold ions. The results of several simulated scans are shown in Figures 9.2 to 9.9 for both protons and gold ions.

**Table I: RHIC parameters**

| Parameter | Protons | Gold Ions |
|-----------|---------|-----------|
| $\beta_{x\min}$ | 1.0m | 1.0m |
| $\beta_{y\min}$ | 1.0m | 1.0m |
| $\epsilon_{x95\%}^N$ | $20\mu$m | $10\mu$m |
| $\epsilon_{y95\%}^N$ | $20\mu$m | $10\mu$m |
| $\sigma_z$ | 0.075m | 0.2m |
| $N_1$ | $1 \times 10^{11}$ | $1 \times 10^9$ |
| $N_2$ | $1 \times 10^{11}$ | $1 \times 10^9$ |
| $N_b$ | 55 | 55 |
| $f_{\rm rev}$ | 78.25kHz | 78.25kHz |
| $\gamma$ | 260 | 108 |
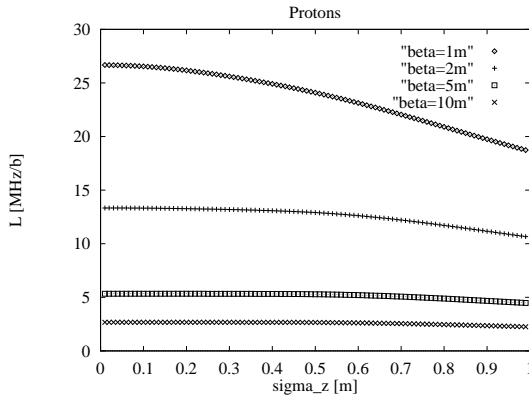


Figure 9.2 Luminosity versus bunch length for proton beams at various $\beta^*$ values.
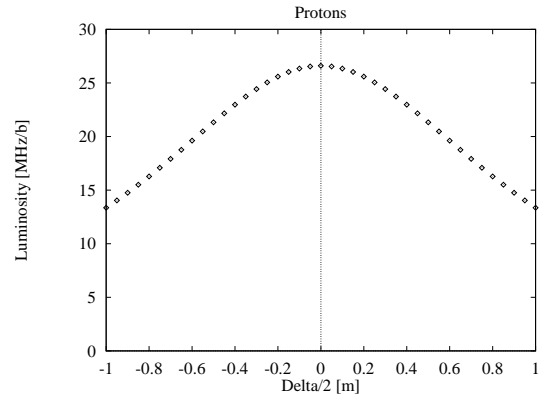
Figure 9.3 Longitudinal scan of luminosity for protons with $\beta^* = 1$m.

Fig. 9.2 shows the variation of the luminosity with bunch length for $\beta^*$ values from 1 to 10 m. Here I have assumed that the beams are round and of the same size

$$\beta_{x1}^* = \beta_{y1}^* = \beta_{x2}^* = \beta_{y2}^* \quad \text{and} \quad \epsilon_{x1}^* = \epsilon_{y1}^* = \epsilon_{x2}^* = \epsilon_{y2}^*. \tag{9.44}$$

This demonstrates the usual rule of thumb that the bunch length should be no larger than the value of $\beta^*$

Fig. 9.5 shows the effect of misalignment of the waist of the the beam. Here I have assumed that the horizontal and vertical waists of both beams are displaced by the same amount but in opposite directions for both rings. This shows that to peak up luminosity, we should measure the optics carefully around the interaction regions. A scan of luminosity versus each waist should be made at some time to ensure that the optics are placing all four waists within about 10 cm of the interaction point.

The pair of beam position monitors (BPM) in each interaction region are separated by about 16.6 m. The beam pipe aperture through the DX and D0 magnets limit the maximum crossing angle to about 1 mr. The alignment of the beams from the BPM's should be better than $200\mu$m, so that we should be able to dead reckon the crossing angle very well, $\theta_{x,y} \leq 6\mu$r. Figs. 9.6 and 9.7 show that there is very little degradation of luminosity for crossing angles up to several hundred microradians. Clearly the longer bunches of the gold beams are a bit more sensitive to crossing angle.

The rf system can easily phase the beams to cross at the required location within a couple of centimeters. Figs. 9.3 and 9.9 show that a $\Delta/2 = 20$cm longitudinal shift of the IP has a marginal effect for both gold and proton beams

Since the BPM system should align the crossing point to a few hundred microns, we should be able to set the beam to collide with at least 30% of the peak luminosity. Even if we miss the crossing point by 0.5 mm, we can perform a two dimensional scan in $100\mu$m steps to get quite close to the peak. Then a finer transverse scan can be performed to reach the peak.
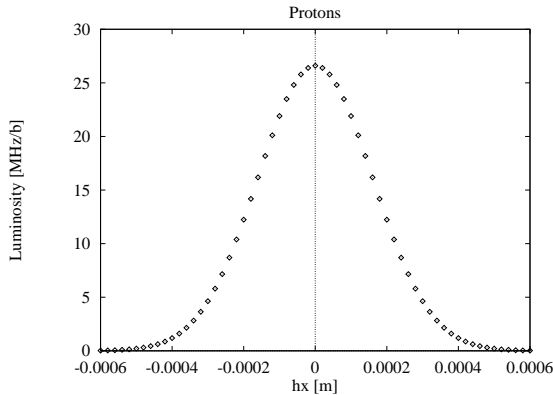


Figure 9.4 Scan of $h_x$ for proton beams at 250 GeV with $\beta^* = 1$m. (The dot spacing is $20\mu$m.)
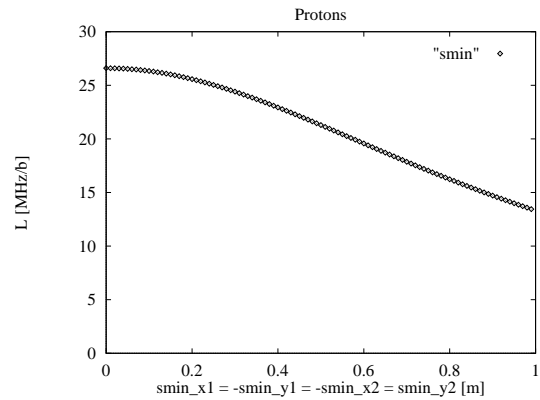


Figure 9.5 Longitudinal scan of beam waists for protons at 250 GeV ($\beta^* = 1$m).

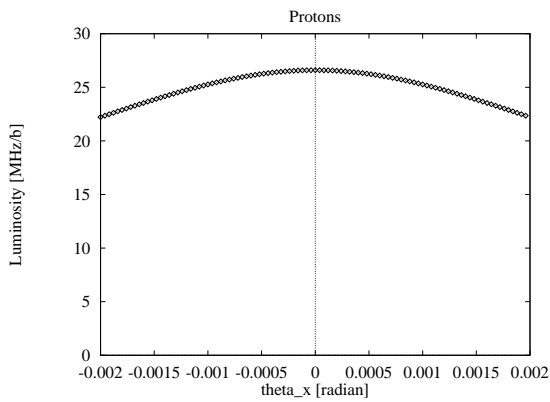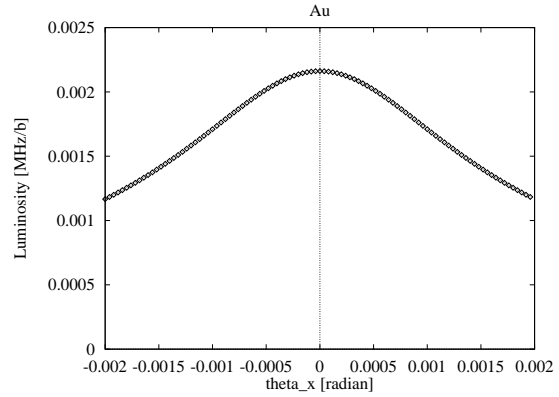Figure 9.6 Scan of $\theta_x$ for proton beams at 250 GeV with $\beta^* = 1$m.



Figure 9.7 Scan of $\theta_x$ for Gold ion beams at 100 GeV/amu with $\beta^* = 1$m and 55 bunches of $10^9$ ions per bunch.
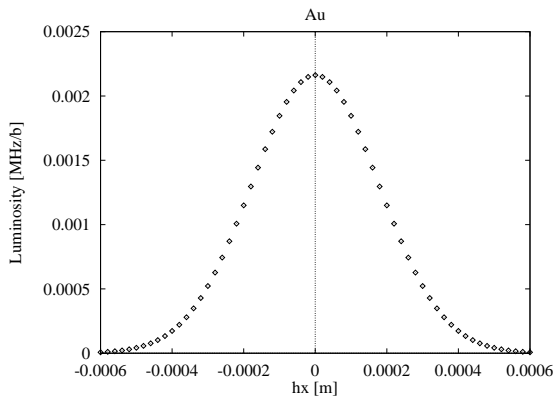


Figure 9.8 Scan of $h_x$ for Gold ion beams at 100 GeV/amu with $\beta^* = 1$m and 55 bunches of $10^9$ ions per bunch. (The dot spacing is $20\mu$m.)



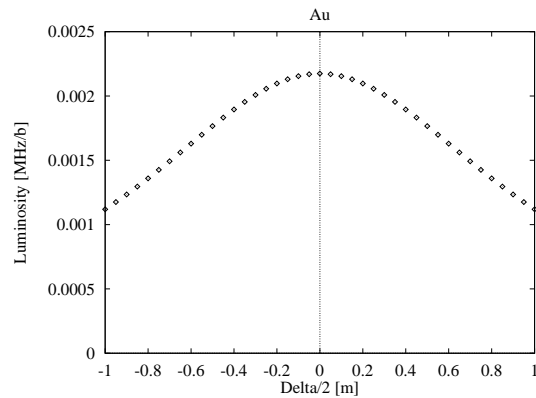Figure 9.9 Longitudinal scan for Gold ion beams at 100 GeV/amu with $\beta^* = 1$m and 55 bunches of $10^9$ ions per bunch.
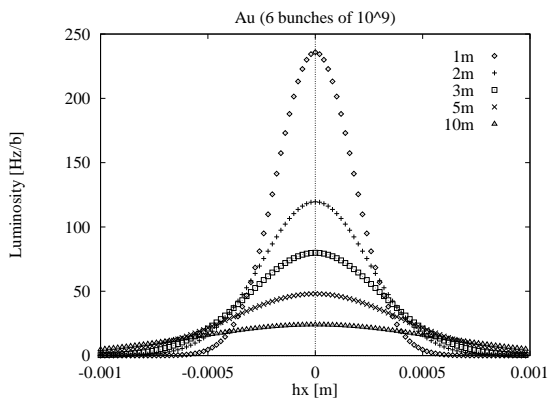


Figure 9.10 Scan of $h_x$ for Gold ion beams at 100 GeV/amu with $\beta^* = 1, 2, 3, 5,$ and 10 m and 6 bunches of $10^9$ ions per bunch. (The dot spacing is $20\mu$m.)
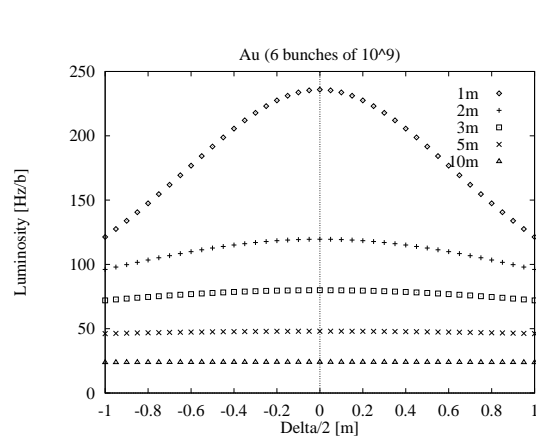


Figure 9.11 Longitudinal scan for Gold ion beams at 100 GeV/amu with $\beta^* = 1, 2, 3, 5,$ and 10 m and 6 bunches of $10^9$ ions per bunch.
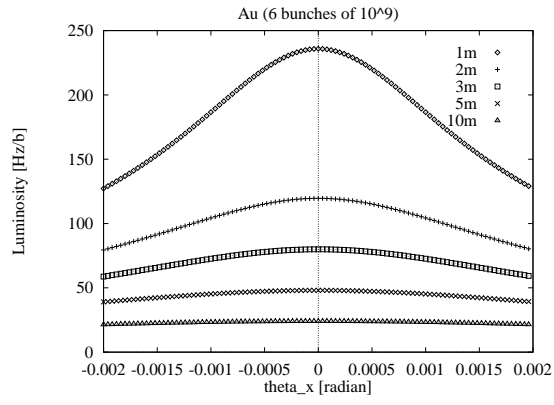
Figure 9.12 Scan of $\theta_x$ for Gold ion beams at 100 GeV/amu with $\beta^* = 1$, 2, 3, 5, and 10 m and 6 bunches of $10^9$ ions per bunch.